

# Bremsstrahlung Cross-Section Formulas and Related Data\*

H. W. KOCH AND J. W. MOTZ

*National Bureau of Standards, Washington, D. C.*

I. Introduction.....	920	IV. Thick-Target Bremsstrahlung Production....	949
II. Bremsstrahlung Cross Sections.....	921	A. Thick-Target Bremsstrahlung Angular	
A. Symbols, Constants, and Energy-Mo-		Distributions.....	949
mentum Relations.....	921	(1) Nonrelativistic and Intermediate	
B. Types of Cross-Section Calculations...	921	Energies.....	949
C. Bremsstrahlung Cross-Section Formulas		(2) Relativistic Energies.....	950
and Classification Diagrams.....	922	B. Thick-Target Bremsstrahlung Spectra..	951
(1) Born-Approximation Cross-Section		(1) Nonrelativistic and Intermediate	
Formulas.....	926	Energies.....	951
(2) Extreme-Relativistic Cross-Section		(2) Relativistic Energies.....	952
Formulas with the Coulomb		C. Efficiency for Bremsstrahlung Production.....	953
Correction.....	927	(1) Nonrelativistic and Intermediate	
D. Graphical Representation of the Form-		Energies.....	955
ulas.....	927	(2) Relativistic Energies.....	955
(1) Dependence of the Bremsstrahlung		(a) Intermediate thickness tar-	
Spectrum on Electron		gets.....	955
Energy.....	929	(b) Thick targets.....	955
(2) Dependence of the Bremsstrahlung		V. Acknowledgments.....	955
Spectrum on Photon Angle	929		
(3) Screening Effects and Coulomb			
Corrections.....	931		
E. Corrections for the Cross-Section For-			
mulas.....	931		
(1) Coulomb Corrections.....	931		
(a) Nonrelativistic energies...	931		
(b) Intermediate energies.....	931		
(c) Extreme-relativistic			
energies.....	932		
(2) High-Frequency-Limit Correc-			
tions.....	933		
(3) Screening Corrections.....	934		
F. Comparison of Theory and Experiment	941		
(1) Cross-Section Differential in Pho-			
ton Energy and Angle.....	942		
(2) Cross-Section Differential in Pho-			
ton Energy.....	942		
(3) Total Cross Section.....	943		
G. Summary.....	946		
III. Electron-Electron Bremsstrahlung.....	947		
A. Maximum Photon Energy.....	947		
B. Cross-Section Formulas for Free Elec-			
trons.....	947		
(1) Nonrelativistic Energies.....	947		
(2) Extreme-Relativistic Energies...	948		
C. Cross-Section Formulas with Binding			
Corrections.....	948		

\* The research reported here was supported jointly by the U. S. Atomic Energy Commission, and by the U. S. Air Force, through the Office of Scientific Research of the Air Research and Development Command.

## I. INTRODUCTION

CONSIDERABLE information about the bremsstrahlung process has accumulated during the past several years. This information includes various cross-section calculations and measurements, which have helped to provide a more accurate description of the process. Unfortunately this material has never been assembled and integrated in an easily referenced form, although some general reviews<sup>1</sup> on the subject are available. This paper provides a coherent summary of the bremsstrahlung cross-section formulas and related data. The theoretical formulas and their specific limitations are presented in a form convenient for practical calculations. Estimates of their accuracy are given for cases where comparisons can be made with experimental results. Correction factors are indicated in either numerical or analytical form. A brief summary of other data pertaining to electron-electron and to thick target bremsstrahlung is also included. No results are presented for electron and photon polarization effects.

Section IIB briefly discusses the problem of making exact cross-section calculations and indicates the general types of calculations that have been completed. A summary of the various cross-section formulas is given in Sec. IIC. Section IID gives useful graphical information derived from the various formulas in IIC. Section IIE lists corrections that can be applied to the above

<sup>1</sup> H. Bethe and E. Salpeter, *Encyclopedia of Physics* (Springer-Verlag, Berlin, 1957), Vol. 35, p. 425; S. T. Stephenson, *ibid.*, Vol. 30, p. 337.

formulas. In Sec. IIF, experimental bremsstrahlung cross sections are compared with the theoretical results contained in Secs. IIC and D. Conclusions with regard to the accuracy of the theory are presented in Sec. IIG. Section III summarizes the very sparse material available on electron-electron bremsstrahlung. Finally, Sec. IV gives a brief treatment of thick target bremsstrahlung with information on the bremsstrahlung angular distributions (IVA), the spectra (IVB), and the production efficiencies (IVC).

II. BREMSSTRAHLUNG CROSS SECTIONS

The cross sections discussed in this section apply to the bremsstrahlung process<sup>2</sup> in which an electron is decelerated in the field of an atomic nucleus. These cross sections give direct estimates of the properties of the radiation emitted when electrons are incident on *thin*<sup>3</sup> targets, and provide basic data for analyzing the *thick* target bremsstrahlung considered in Sec. IV.

A. Symbols, Constants, and Energy-Momentum Relations

- $E_0, E$  = initial and final total energy of the electron in a collision, in  $m_0c^2$  units.†
- $\mathbf{p}_0, \mathbf{p}$  = initial and final momentum of the electron in a collision, in  $m_0c$  units.
- $T_0, T$  = initial and final kinetic energy of the electron in a collision, in  $m_0c^2$  units.†
- $k, \mathbf{k}$  = energy and momentum of the emitted photon, in  $m_0c^2$  and  $m_0c$  units.†
- $\mathcal{E}_0$  = total energy of an electron incident on a thick target, in  $m_0c^2$  units.†
- $\mathcal{T}_0$  = kinetic energy of an electron incident on a thick target, in  $m_0c^2$  units.†
- $\theta_0, \theta$  = angles of  $\mathbf{p}_0$  and  $\mathbf{p}$  with respect to  $\mathbf{k}$ .
- $\phi$  = angle between the planes  $(\mathbf{p}_0, \mathbf{k})$  and  $(\mathbf{p}, \mathbf{k})$ .
- $d\Omega_k$  = element of solid angle,  $\sin\theta_0 d\theta_0 d\phi$ , in the direction of  $\mathbf{k}$ .
- $d\Omega_p$  = element of solid angle,  $\sin\theta d\theta d\phi$ , in the direction of  $\mathbf{p}$ .
- $\mathbf{q}$  = momentum transferred to the nucleus, in  $m_0c$  units.  
 $= \mathbf{p}_0 - \mathbf{p} - \mathbf{k}; q^2 = p_0^2 + p^2 + k^2 - 2p_0k \cos\theta_0 + 2pk \cos\theta - 2p_0p(\cos\theta \cos\theta_0 + \sin\theta \sin\theta_0 \cos\phi)$ .
- $\beta_0, \beta$  = ratio of the initial and final electron velocity in a collision to the velocity of light.

- $Z$  = atomic number of target material.
- $d\sigma_j$  = bremsstrahlung cross section, differential with respect to the parameter  $j$ , in units of  $\text{cm}^2$  per atom per incident electron.
- $d\tau$  = volume element.
- $\mathbf{r}$  = radius vector from a center, in units of the Compton wavelength,  $\lambda_0$ .
- $\alpha$  = angle of  $\mathbf{k}$  with respect to the direction of the electron beam incident on a thick target.

- $N_0$  =  $6.03 \times 10^{23}$  atoms (or molecules) per mole.
- $c$  =  $3.00 \times 10^{10}$  cm per sec.
- $e$  =  $4.80 \times 10^{-10}$  esu =  $1.60 \times 10^{-19}$  coulomb.
- $e^2$  =  $1.44 \times 10^{-13}$  Mev cm.
- $\hbar$  =  $h/2\pi = 6.58 \times 10^{-22}$  Mev sec =  $1.05 \times 10^{-27}$  erg sec.
- $\hbar c$  = 12.4 kev-angstroms.
- $\hbar c$  =  $1.97 \times 10^{-11}$  Mev cm.
- $\hbar c/e^2$  = 137.
- $m_0$  =  $9.11 \times 10^{-28}$  g (electron mass).
- $m_0c^2$  = 0.511 Mev.
- $\lambda_0$  =  $\hbar/m_0c = 3.86 \times 10^{-11}$  cm (Compton wavelength).
- $r_0$  =  $e^2/m_0c^2 = \lambda_0/137 = 2.82 \times 10^{-13}$  cm (classical electron radius).
- $\bar{\phi}$  =  $Z^2 r_0^2 / 137 = Z^2 5.78 \times 10^{-28}$   $\text{cm}^2$ .
- $a_0$  =  $\hbar^2/m_0e^2 = 0.530 \times 10^{-8}$  cm (radius of hydrogen atom).  
 $= 137\lambda_0 = (137)^2 r_0$
- $\phi_0$  =  $8\pi r_0^2/3$  (Thomson formula) =  $6.64 \times 10^{-25}$   $\text{cm}^2$ .
- $e^2/a_0$  =  $2I_0 = 27.2$  ev.
- $I_0$  = ionization energy of hydrogen atom =  $1/2(137)^2$  in  $m_0c^2$  units.
- $Z^2 I_0$  = ionization energy of  $K$  electron (*if*  $\ll 1$ ).
- 1 Mev =  $1.60 \times 10^{-6}$  erg.

$E_0^2 = p_0^2 + 1, E^2 = p^2 + 1.$   
 $E_0 = T_0 + 1, E = T + 1.$

$E_0 = \frac{1}{(1-\beta_0^2)^{\frac{1}{2}}}, E = \frac{1}{(1-\beta^2)^{\frac{1}{2}}}$

$E_0 = k + E.$

$p_0 = [T_0(T_0 + 2)]^{\frac{1}{2}}, p = [T(T + 2)]^{\frac{1}{2}}$

$p_0 = \frac{\beta_0}{(1-\beta_0^2)^{\frac{1}{2}}}, p = \frac{\beta}{(1-\beta^2)^{\frac{1}{2}}}$

$\beta_0 = \frac{p_0}{E_0}, \beta = \frac{p}{E}$

B. Types of Cross-Section Calculations

The bremsstrahlung cross section  $d\sigma$ , for single photon emission in a large cubic box of side  $L$ , is given by the transition probability per atom per electron divided by the incoming electron velocity. This cross section

<sup>2</sup> Except for electron-electron bremsstrahlung which is briefly considered in Sec. III, no results are presented for other bremsstrahlung processes, involving for example the acceleration of positrons or protons.

<sup>3</sup> A target is defined to be thin if both the electron scattering and energy loss processes have a negligible influence on the energy and angular distributions of the bremsstrahlung. Order of magnitude estimates of such thin targets for particular energy regions can be found in the references listed in Sec. IIG.

† This system of units for the symbols is used consistently throughout this paper. For cases in which the data are given in Mev units, these symbols have the multiplicative factor 0.51; for example, the kinetic energy in Mev units is represented by the quantity  $0.51T_0$ .

can be expressed in dimensions of  $\text{cm}^2$  as

$$d\sigma = \frac{w}{(p_0c/E_0)} \left( \frac{\hbar}{m_0c} \right)^3 L^3, \quad (\text{II-1})$$

where

$$w = (2\pi/\hbar)\rho_f |H_{if}|^2. \quad (\text{II-2})$$

The term  $\rho_f$  is the density of final states and can be written as

$$\rho_f = \frac{pEk^2dkd\Omega_k d\Omega_p L^6}{(2\pi)^6 m_0c^2}. \quad (\text{II-3})$$

The term  $H_{if}$  is the matrix element for the transition of the system from an initial state before the emission of the photon to a final state after the emission. The quantity  $|H_{if}|^2$  in formula (II-2) can be written as

$$|H_{if}|^2 = \left( \frac{2\pi e^2}{k \hbar c} \right) (m_0c^2)^2 \times \left| \int \psi_f^*(\lambda^* \cdot \alpha) e^{-ik \cdot r} \psi_i d\tau \right|^2 L^{-9}. \quad (\text{II-4})$$

In the foregoing,  $\lambda$  is the unit polarization vector of the photon,  $\alpha$  is the Dirac matrix, and  $\psi_i$  and  $\psi_f$  are the Dirac wave functions for the initial and final electrons, respectively. Therefore the cross section in  $\text{cm}^2$  can be written as

$$d\sigma = \frac{137r_0^2}{(2\pi)^4} \frac{pE_0E}{p_0} \left| \int \psi_f^*(\lambda^* \cdot \alpha) e^{-ik \cdot r} \psi_i d\tau \right|^2 \times kdkd\Omega_k d\Omega_p. \quad (\text{II-5})$$

The important quantity to be evaluated is the matrix element  $H_{if}$ , defined in formula (II-4).

The problem of evaluating an "exact" expression for the cross section involves, therefore, the use in the matrix element of "exact" wave functions, which describe an electron in a screened, nuclear Coulomb field. It is not possible to solve the Dirac wave equation in closed form for an electron in a Coulomb field, primarily because the wave function must be represented as an infinite series.<sup>4</sup> Therefore, various approximate wave functions and procedures have been used.

The cross-section calculations that have been made may be classified either as nonrelativistic or relativistic depending on whether the Schrödinger or Dirac form of the Hamiltonian is used for the electron and field system. The calculations have been carried out with (a) nonrelativistic Coulomb wave functions (Sommerfeld); (b) relativistic Coulomb wave functions (Sommerfeld-Maue) valid to first order in  $(Z/137)^2/l$ , where  $l$  is the angular momentum quantum number that is the summation index in the expansion of the wave function;

<sup>4</sup> A detailed discussion of this problem is given by H. A. Bethe and L. C. Maximon, *Phys. Rev.* **93**, 768 (1954).

and (c) free-particle wave functions perturbed to first order in  $Z$  (Born-approximation procedure).

The nonrelativistic cross-section formulas derived in the dipole approximation by Sommerfeld<sup>5</sup> with Coulomb wave functions have a complicated form with hypergeometric functions and are difficult to evaluate. Some numerical estimates<sup>6</sup> of the Sommerfeld cross sections have been made for selected values of the electron energy, the target atomic number, and the photon energy. However, the theory is only valid when  $\beta_0$  is small compared to unity, and can be expected to break down for initial electron energies greater than a few kilovolts. In addition, the theory disregards screening effects, which are important for very low energies and for targets with high atomic numbers. Because of these limitations, results of the Sommerfeld theory are not presented here.

Cross-section calculations with relativistic Coulomb wave functions (Sommerfeld-Maue) including screening corrections have been made by Olsen, Maximon, and Wergeland<sup>7</sup> and by Olsen and Maximon.<sup>8</sup> Their formulas are valid only in the extreme-relativistic region (above 50 Mev). Their results have the form of an additive correction factor to the Born-approximation formulas.

The cross-section formulas calculated by the Born-approximation procedure with free-particle wave functions are available in a relatively simple analytical form for nonrelativistic and relativistic energies, with or without screening. In general, the Born approximation theory becomes less reliable as (a) the atomic number of the target increases, (b) the initial electron energy decreases, and (c) the photon energy approaches the high-frequency limit. In spite of their limited validity, the Born-approximation formulas have been surprisingly successful in predicting the properties of the bremsstrahlung radiation. Even where there is a breakdown of the Born approximation, the accuracy of the cross-section formulas is still reasonably good, and in the worst cases (except at the high-frequency limit), they can be expected to give at least the correct order of magnitude. Therefore, this paper emphasizes the Born-approximation cross-section formulas and includes various theoretical and empirical corrections to these formulas. Detailed references to the many papers in which these formulas are derived are given in Table III.

### C. Bremsstrahlung Cross-Section Formulas and Classification Diagrams

A general classification of the various differential forms of the bremsstrahlung cross section is presented in Chart 1 for the Born-approximation formulas and in Chart 2 for the extreme-relativistic formulas that con-

<sup>5</sup> A. Sommerfeld, *Wellenmechanik* (Frederick Ungar, New York, 1950), Chap. 7.

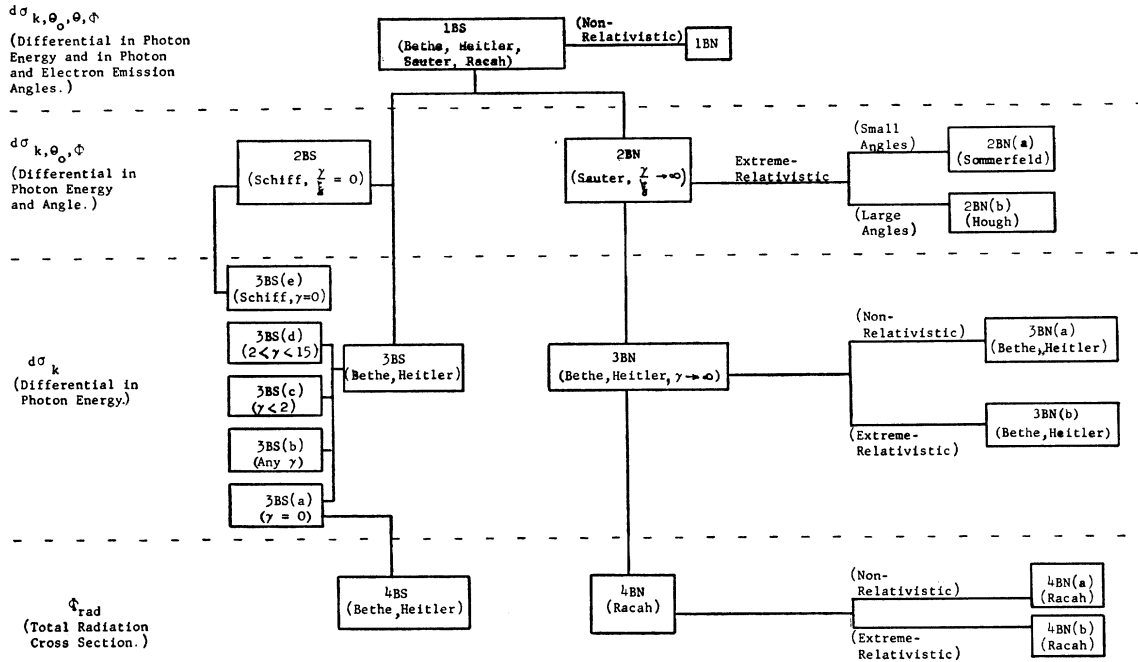
<sup>6</sup> P. Kirkpatrick and L. Wiedmann, *Phys. Rev.* **67**, 321 (1945).

<sup>7</sup> Olsen, Maximon, and Wergeland, *Phys. Rev.* **106**, 27 (1957).

<sup>8</sup> H. Olsen and L. C. Maximon, *Phys. Rev.* **114**, 887 (1959).

CHART 1

Born Approximation Cross Section Formulas



tain the Coulomb correction. The formulas represented are summed over the directions of the electron spin and the photon polarization vectors, and thus do not include all of the possible differential forms of the cross section. The primary formula gives the cross section that is differential in photon energy and in photon and electron emission angles. The remaining formulas that branch out from this starting point are divided into two main groups that are designated as screened or non-screened. Further subdivisions are made; these depend on the type of screening approximation, and on whether nonrelativistic, extreme-relativistic, small-angle, or large-angle approximations are used. For most of the cases, the charts include the names of the principal authors associated with a particular formula.

The formulas are identified as follows: (a) the number applies to a particular differential form of the cross section; (b) the first letter indicates either B for Born approximation (Chart 1) or C for Coulomb correction (Chart 2); (c) the second letter indicates either S for screening or N for no screening; and (d) the last letter a, b, or c indicates further subdivisions for specific approximations. The following notation has been adopted here. The differential forms of the bremsstrahlung cross section are designated by the symbol,  $d\sigma_{\alpha,\beta,\dots}$ . This symbol is the bremsstrahlung cross section that is differential only with respect to the parameters given by the subscripts  $\alpha, \beta, \dots$ , and is explicitly defined by  $d\sigma_{\alpha,\beta,\dots} \equiv (d^n\sigma/d\alpha d\beta \dots) d\alpha d\beta \dots$ . The

unit of the cross section,  $d\sigma_{\alpha,\beta,\dots}$ , is  $\text{cm}^2$  per atom per incident electron.

The symbols and definitions for the specific cross sections are as follows.

(a)  $d\sigma_{k,\theta_0,\theta,\phi}$  is the bremsstrahlung cross section that is differential with respect to the photon energy,  $k$ , and to the photon and electron emission angles,  $\theta_0, \theta$ , and  $\phi$ . This formula contains the parameters  $E_0, Z, k, \theta_0, \theta$ , and  $\phi$ .

CHART 2

Extreme-Relativistic Cross Section Formulas with Coulomb Correction

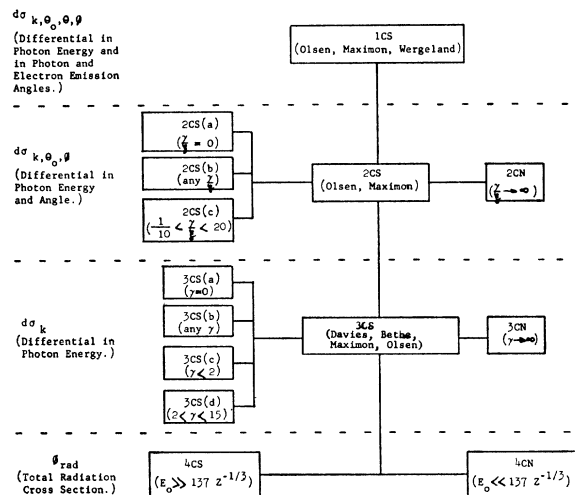


TABLE I. Born-approximation cross-section formulas.

**Formula 1BS**—Differential in photon energy and in photon and electron emission angles.

Approximation (H). Reference formulas: (13) in reference (a), (2) in reference (b), (13) in reference (c), (29) in reference (e).

$$d\sigma_{k,\theta_0,\phi} = \frac{Z^2}{137} \left( \frac{r_0}{2\pi} \right)^2 [1 - F(q, Z)]^2 \frac{dk}{k} \frac{p}{p_0} \frac{d\Omega_k d\Omega_p}{q^4} \left\{ \frac{p^2 \sin^2\theta}{(E - p \cos\theta)^2} (4E_0^2 - q^2) + \frac{p_0^2 \sin^2\theta_0}{(E_0 - p_0 \cos\theta_0)^2} (4E^2 - q^2) \right. \\ \left. - \frac{2p p_0 \sin\theta \sin\theta_0 \cos\phi (4EE_0 - q^2)}{(E - p \cos\theta)(E_0 - p_0 \cos\theta_0)} + \frac{2k^2 (p^2 \sin^2\theta + p_0^2 \sin^2\theta_0 - 2p p_0 \sin\theta \sin\theta_0 \cos\phi)}{(E - p \cos\theta)(E_0 - p_0 \cos\theta_0)} \right\},$$

where

$$q^2 = p^2 + p_0^2 + k^2 - 2p_0 k \cos\theta_0 + 2pk \cos\theta - 2p_0 p (\cos\theta \cos\theta_0 + \sin\theta \sin\theta_0 \cos\phi)$$

and  $F(q, z)$  = atomic form factor discussed in Sec. IIE(3).

**Formula 1BN**—Differential in photon energy and in photon and electron emission angles.

Approximations (H), (B), (I). Reference formula (17) in reference (c).

$$d\sigma_{k,\theta_0,\phi} = \frac{Z^2}{137} \left( \frac{r_0}{\pi} \right)^2 \frac{dk}{k} \frac{p}{p_0} \frac{d\Omega_k d\Omega_p}{q^4} \{ p^2 \sin^2\theta + p_0^2 \sin^2\theta_0 - 2p p_0 \sin\theta \sin\theta_0 \cos\phi \},$$

where

$$q^2 = p^2 + p_0^2 - 2p p_0 (\cos\theta \cos\theta_0 + \sin\theta \sin\theta_0 \cos\phi).$$

**Formula 2BS**—Differential in photon energy and angle.

Approximations (H), (G), (M), (J), (K). Reference formula (1) in reference (h).

$$d\sigma_{k,\theta_0} = \frac{4Z^2 r_0^2}{137} \frac{dk}{k} y dy \left\{ \frac{16y^2 E}{(y^2 + 1)^4 E_0} \frac{(E_0 + E)^2}{(y^2 + 1)^2 E_0^2} + \left[ \frac{E_0^2 + E^2}{(y^2 + 1)^2 E_0^2} - \frac{4y^2 E}{(y^2 + 1)^4 E_0} \right] \ln M(y) \right\},$$

where

$$y = E_0 \theta_0, \quad \frac{1}{M(y)} = \left( \frac{k}{2E_0 E} \right)^2 + \left( \frac{Z^4}{111(y^2 + 1)} \right)^2.$$

Comment: This formula becomes Formula 2BN(a) when  $Z=0$  in  $M(y)$ .

**Formula 2BN**—Differential in photon energy and angle.

Approximations (H), (B). Reference formulas: (11) in reference (d), (4.1) in reference (f).

$$d\sigma_{k,\theta_0,\phi} = \frac{Z^2 r_0^2}{8\pi 137} \frac{dk}{k} \frac{p}{p_0} \frac{d\Omega_k}{\Delta_0^4} \left\{ \frac{8 \sin^2\theta_0 (2E_0^2 + 1)}{p_0^2 \Delta_0^4} - \frac{2(5E_0^2 + 2EE_0 + 3)}{p_0^2 \Delta_0^2} - \frac{2(p_0^2 - k^2)}{Q^2 \Delta_0^2} + \frac{4E}{p_0^2 \Delta_0} \right. \\ \left. + \frac{L}{p_0 p} \left[ \frac{4E_0 \sin^2\theta_0 (3k - p_0^2 E)}{p_0^2 \Delta_0^4} + \frac{4E_0^2 (E_0^2 + E^2)}{p_0^2 \Delta_0^2} - \frac{2 - 2(7E_0^2 - 3EE_0 + E^2)}{p_0^2 \Delta_0^2} + \frac{2k(E_0^2 + EE_0 - 1)}{p_0^2 \Delta_0} \right] \right. \\ \left. - \left( \frac{4\epsilon}{p \Delta_0} \right) + \left( \frac{\epsilon^Q}{p Q} \right) \left[ \frac{4}{\Delta_0^2} - \frac{6k}{\Delta_0} - \frac{2k(p_0^2 - k^2)}{Q^2 \Delta_0} \right] \right\},$$

where

$$L = \ln \left[ \frac{EE_0 - 1 + p p_0}{EE_0 - 1 - p p_0} \right]; \quad \Delta_0 = E_0 - p_0 \cos\theta_0; \quad \epsilon = \ln \left[ \frac{E + p}{E - p} \right]; \quad \epsilon^Q = \ln \left[ \frac{Q + p}{Q - p} \right]$$

$$Q^2 = p_0^2 + k^2 - 2p_0 k \cos\theta_0.$$

**Formula 2BN(a)**—Differential in photon energy and angle.

Approximations (H), (B), (J), (K).

$$d\sigma_{k,\theta_0,\phi} = \frac{2Z^2 r_0^2}{\pi 137} \frac{E}{E_0} \frac{dk}{k} \frac{d\Omega_k}{k} \left\{ \frac{16(\theta_0 E_0)^2 E_0^2}{(1 + \theta_0^2 E_0^2)^4} - \frac{(E_0 + E)^2 E_0}{E(1 + \theta_0^2 E_0^2)^2} + 2 \ln \left( \frac{EE_0}{k} \right) \left[ \frac{(E^2 + E_0^2) E_0}{E(1 + \theta_0^2 E_0^2)^2} - \frac{4\theta_0^2 E_0^4}{(1 + \theta_0^2 E_0^2)^4} \right] \right\}.$$

Comment: This formula was obtained from formula 2BN by making the high-energy and small-angle approximations. The same result is obtainable from formula 2BS by setting  $Z=0$  in  $M(y)$ .

**Formula 2BN(b)**—Differential in photon energy and angle.

Approximations (H), (B), (J), (L). Reference formula (8) in reference (i).

$$d\sigma_{k,\theta_0,\phi} = \frac{Z^2 r_0^2}{4\pi 137} \frac{E}{E_0^3} \frac{dk}{k} \frac{d\Omega_k}{(1 - \cos\theta_0)^2} \left\{ \left( \frac{E_0^2 + E^2}{EE_0} \right) \sin^2\theta_0 \ln \frac{2E_0 E}{k} - \frac{(5E_0 + 2E)}{E_0} + \frac{2[E^2 - 2E_0^2 \ln(k/E_0)]}{E_0 E} [1 - \cos\theta_0] \right. \\ \left. - \frac{E[Q^2 + E(k - E_0 \cos\theta_0)]}{E_0 Q^2 (1 - \cos\theta_0)} - \frac{E_0 k (1 - \cos\theta_0)}{E Q^3} [3Q^2 + E(E_0 + k)] \ln \left( \frac{Q + E}{Q - E} \right) \right\}$$

where

$$Q^2 = E^2 + 2kE_0(1 - \cos\theta_0),$$

TABLE I.—(Continued).

**Formula 3BS**—Differential in photon energy.

Approximations (H), (J). Reference formulas: (31), (34), (35) in reference (a); (62) in reference (b); (21), (26) in reference (c); (56)–(58b) in reference (j).

$$d\sigma_k = \frac{4Z^2 r_0^2 dk}{137 k} \left\{ \left( 1 + \left( \frac{E}{E_0} \right)^2 \right) \left[ \frac{\phi_1(\gamma)}{4} - \frac{1}{3} \ln Z \right] - \frac{2 E}{3 E_0} \left[ \frac{\phi_2(\gamma)}{4} - \frac{1}{3} \ln Z \right] \right\}.$$

**Formula 3BS(a)**—Complete screening ( $\gamma=0$  or  $\phi_1(\gamma=0)=4 \ln 183$ ;  $\phi_2(\gamma=0)=\phi_1(\gamma=0)-\frac{2}{3}$ ).  
Formula 3BS with  $\gamma=0$ .

$$d\sigma_k = \frac{4Z^2 r_0^2 dk}{137 k} \left\{ \left[ 1 + \left( \frac{E}{E_0} \right)^2 - \frac{2 E}{3 E_0} \right] \ln(183Z^{-1}) + \frac{1 E}{9 E_0} \right\}.$$

**Formula 3BS(b)**—Arbitrary screening.

$$d\sigma_k = \frac{4Z^2 r_0^2 dk}{137 k} \left\{ \left( 1 + \left( \frac{E}{E_0} \right)^2 \right) \left[ \int_{\delta}^1 (q-\delta)^2 (1-F(q))^2 \frac{dq}{q^3} + 1 \right] - \frac{2 E}{3 E_0} \left[ \int_{\delta}^1 \left( q^2 - 6\delta^2 q \ln \frac{q}{\delta} + 3\delta^2 q - 4\delta^3 \right) (1-F(q))^2 \frac{dq}{q^4} + \frac{5}{6} \right] \right\},$$

where

$$\delta = k / (2E_0E).$$

**Formula 3BS(c)**—Intermediate screening I ( $\gamma < 2$ ).

Formula 3BS with  $\phi_1(\gamma)$  and  $\phi_2(\gamma)$  given in Fig. 1.

**Formula 3BS(d)**—Intermediate screening II ( $2 < \gamma < 15$ ).

Formula 3BS with  $\phi_1(\gamma) = \phi_2(\gamma) = 19.19 - 4 \ln \gamma - 4c(\gamma)$  with  $c(\gamma)$  given in Fig. 2.

$$d\sigma_k = \frac{4Z^2 r_0^2 dk}{137 k} \left[ 1 + \left( \frac{E}{E_0} \right)^2 - \frac{2 E}{3 E_0} \right] \left[ \ln \frac{2E_0E}{k} - \frac{1}{3} - c(\gamma) \right].$$

**Formula 3BS(e)**—Differential in photon energy.

Approximations (H), (G), (M), (J). Reference formula (3) in reference (h).

$$d\sigma_k = \frac{2Z^2 r_0^2 dk}{137 k} \left\{ \left( 1 + \left( \frac{E}{E_0} \right)^2 - \frac{2 E}{3 E_0} \right) \left( \ln M(0) + 1 - \frac{2}{b} \tan^{-1} b \right) + \frac{E}{E_0} \left[ \frac{2}{b^2} \ln(1+b^2) + \frac{4(2-b^2)}{3b^2} \tan^{-1} b - \frac{8}{3b^2} + \frac{2}{9} \right] \right\},$$

where

$$b = \left( \frac{2E_0EZ^1}{111k} \right); \quad \frac{1}{M(0)} = \left( \frac{k}{2E_0E} \right)^2 + \left( \frac{Z^1}{111} \right)^2.$$

Comment: This formula is obtained from formula 50 of reference (b).

**Formula 3BN**—Differential in photon energy.

Approximations (H), (B). Reference formulas: (15) in reference (a), (16) in reference (c), (17) in reference (d), (37) in reference (e).

$$d\sigma_k = \frac{Z^2 r_0^2 dk}{137 k} \frac{p}{p_0} \left\{ \frac{4}{3} - 2E_0E \left( \frac{p^2 + p_0^2}{p^2 p_0^2} \right) + \frac{\epsilon_0 E}{p_0^3} + \frac{\epsilon E_0}{p^3} + \frac{\epsilon \epsilon_0}{p_0 p} + L \left[ \frac{8E_0E}{3p_0 p} + \frac{k^2(E_0^2 E^2 + p_0^2 p^2)}{p_0^3 p^3} + \frac{k}{2p_0 p} \left( \left( \frac{E_0E + p_0^2}{p_0^3} \right) \epsilon_0 - \left( \frac{E_0E + p^2}{p^3} \right) \epsilon + \frac{2kE_0E}{p^2 p_0^2} \right) \right] \right\},$$

where

$$L = 2 \ln \left[ \frac{E_0E + p_0 p - 1}{k} \right]; \quad \epsilon_0 = \ln \left( \frac{E_0 + p_0}{E_0 - p_0} \right); \quad \epsilon = \ln \left( \frac{E + p}{E - p} \right).$$

**Formula 3BN(a)**—Differential in photon energy.

Approximations (H), (B), (I). Reference formula (18) in reference (c).

$$d\sigma_k = \frac{Z^2 r_0^2 16 dk}{137 3 k} \frac{1}{p_0^2} \ln \left( \frac{p_0 + p}{p_0 - p} \right).$$

**Formula 3BN(b)**—Differential in photon energy.

Approximations (H), (B), (J). Reference formulas: (16) in reference (a), (21) in reference (c), (56) in reference (j).

$$d\sigma_k = \frac{4Z^2 r_0^2 dk}{137 k} \left[ 1 + \left( \frac{E}{E_0} \right)^2 - \frac{2 E}{3 E_0} \right] \left[ \ln \left( \frac{2E_0E}{k} \right) - \frac{1}{3} \right].$$

Comment: This formula results directly from Formula 3BS(e) when  $b \rightarrow 0$  and from formula 3BS when  $\gamma \rightarrow \infty$ .

TABLE I.—(Continued).

**Formula 4BS**—Total radiation cross section.

Approximations (H), (F), (J). Reference formulas: (47) in reference (a), (34) in reference (c), (62) in reference (j).

$$\phi_{\text{rad}} = \frac{4Z^2 r_0^2}{137} \left[ \ln(183Z^{-1}) + \frac{1}{18} \right].$$

**Formula 4BN**—Total radiation cross section.

Approximations (H), (C). Reference formulas: (29) in reference (c), (41) in reference (e).

$$\phi_{\text{rad}} = \frac{Z^2 r_0^2}{137} \left\{ \frac{(12E_0^2 + 4)}{3E_0 p_0} \ln(E_0 + p_0) - \frac{(8E_0 + 6p_0)}{3E_0 p_0^2} [\ln(E_0 + p_0)]^2 - \frac{2}{E_0 p_0} [F(x)] \right\},$$

where

$$F(x) = \int_0^x \frac{\ln(1+y)}{y} dy \quad \text{and} \quad x = 2p_0(E_0 + p_0).$$

For small  $x$ ,  $F$  can be expanded in the power series:

$$F(x) = x - \frac{x^2}{4} + \frac{x^3}{9} - \frac{x^4}{16} + \dots$$

For large  $x$ ,  $F$  is given by

$$F(x) = \frac{1}{2}\pi^2 + \frac{1}{2}(\ln x)^2 - F(1/x).$$

**Formula 4BN(a)**—Total radiation cross section.

Approximations (H), (C), (I). Reference formulas: (32) in reference (c), (21) in reference (d).

$$\phi_{\text{rad}} = (16/3)(Z^2 r_0^2 / 137).$$

**Formula 4BN(b)**—Total radiation cross section.

Approximations (H), (C), (J). Reference formulas: (33) in reference (c), (41') in reference (e), (61) in reference (j), (46) in (a), (22) in (d).

$$\phi_{\text{rad}} = \frac{4Z^2 r_0^2}{137} (\ln 2E_0 - \frac{1}{3}).$$

(b)  $d\sigma_{k,\theta_0,\phi}$  is the bremsstrahlung cross section that is differential with respect to the photon energy,  $k$ , and the emission angles  $\theta_0$  and  $\phi$ . It can be obtained by integrating the differential cross section in (a) over the direction of the outgoing electron. This formula contains the parameters  $E_0$ ,  $Z$ ,  $k$ , and  $\theta_0$ .

(c)  $d\sigma_k$  is the bremsstrahlung cross section that is differential with respect to the photon energy  $k$ . It can be obtained by integrating the differential cross section in (a) over the emission directions of the photon and the electron. This formula contains the parameters  $E_0$ ,  $Z$ , and  $k$ .

(d)  $\phi_{\text{rad}}$  is the only cross-section symbol used here that does not represent a differential form of the bremsstrahlung cross section. It is equal to the quantity,  $(1/E_0) \int_0^{T_0} k d\sigma_k$ . This form of a total bremsstrahlung cross section integrated over photon energy and photon and electron emission angles was introduced by Heitler,<sup>9</sup> who has defined it as the cross section for the energy lost by radiation. This formula contains the parameters  $E_0$  and  $Z$ .

The Born-approximation formulas that apply to Chart 1 are presented in Table I, and the extreme-relativistic formulas with the Coulomb correction that apply to Chart 2 are presented in Table II. The im-

portant references and approximations for the formulas in Tables I and II are listed in Table III. The explicit expressions for the formulas in Tables I and II are not necessarily the same as the formulas in the original references because the attempt is made to use consistent units and symbols, with energies and momenta expressed in  $m_0c^2$  and  $m_0c$  units, respectively.

#### (1) Born-Approximation Cross-Section Formulas

The Born-approximation calculations require the initial and final electron kinetic energies in a collision to be large enough to satisfy the conditions:  $(2\pi Z/137\beta_0)$ ,  $(2\pi Z/137\beta) \ll 1$ . At extreme-relativistic energies, the cross sections predicted by the Born-approximation formulas are larger than the true cross sections. For example, the value of the total cross section predicted for lead by the Born-approximation formula is about 10% larger than the value predicted by more accurate formulas.<sup>7</sup> At very low energies, the situation is reversed and the Born-approximation cross section is smaller than the true cross section. The energy region in which the Born-approximation formulas require only small corrections is approximately between 4 and 10 Mev for the initial electron kinetic energy. As a rough guide, it is estimated that Born-approximation formulas for the total radiation cross section,  $\phi_{\text{rad}}$ , are correct to within 10% for initial electron kinetic energies above 2 Mev and within a factor of two below 2 Mev.

<sup>9</sup> W. Heitler, *The Quantum Theory of Radiation* (Oxford University Press, London, 1954), third edition, p. 242.

(2) *Extreme-Relativistic Cross-Section Formulas with the Coulomb Correction*

The formulas in Table II are valid for arbitrary  $Z$  and have been developed in a series of papers by Bethe and Maximon,<sup>10</sup> Olsen,<sup>11</sup> Olsen, Maximon and Wergeland,<sup>7</sup> Olsen and Maximon,<sup>8,12</sup> and Davies, Bethe, and Maximon.<sup>13</sup> Their calculations were carried out (a) with Sommerfeld-Maue wave functions, and (b) with the extreme relativistic approximations:  $E_0, E, k \gg 1$ , and  $p_0 \theta_0 \sim 1$ . These formulas are estimated<sup>10</sup> to have an accuracy of the order of  $(Z/137)^2 (\ln E/E)$  which is

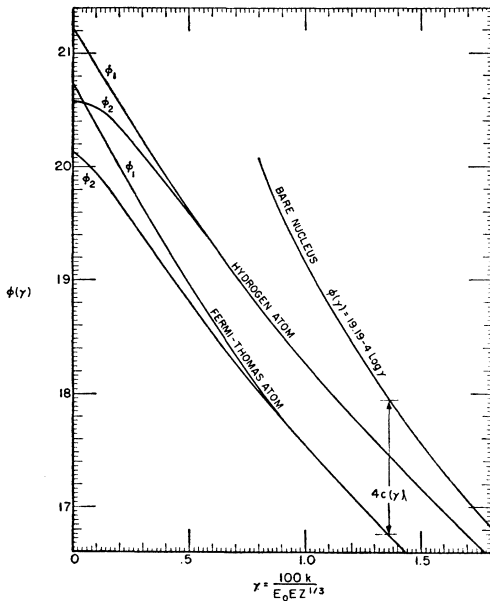


FIG. 1. Screening factors,<sup>28</sup>  $\phi_1(\gamma)$  and  $\phi_2(\gamma)$ , for electron-nuclear bremsstrahlung plotted as a function of  $\gamma = 100k/E_0EZ^{1/3}$ . The curve marked "Hydrogen atom" was calculated<sup>41</sup> with exact wave functions. The curves for the Thomas-Fermi atom and a bare nucleus differ by the quantity  $4c(\gamma)$ , where the function  $c(\gamma)$  is plotted in Fig. 2.

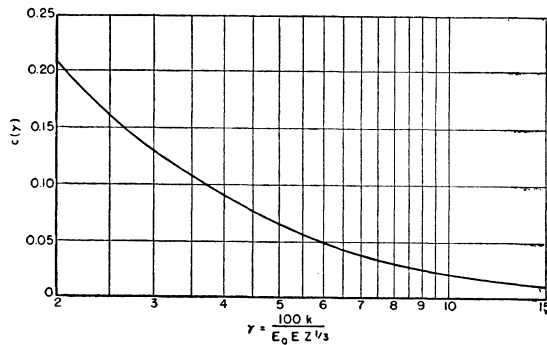


FIG. 2. Screening factor,<sup>28</sup>  $c(\gamma)$ , for electron-nuclear bremsstrahlung plotted as a function of  $\gamma = 100k/E_0EZ^{1/3}$ .

<sup>10</sup> H. Bethe and L. C. Maximon, Phys. Rev. **93**, 768 (1954).  
<sup>11</sup> H. Olsen, Phys. Rev. **99**, 1335 (1955).  
<sup>12</sup> H. Olsen and L. C. Maximon, Phys. Rev. **110**, 589 (1958).  
<sup>13</sup> Davies, Bethe, and Maximon, Phys. Rev. **93**, 788 (1954).

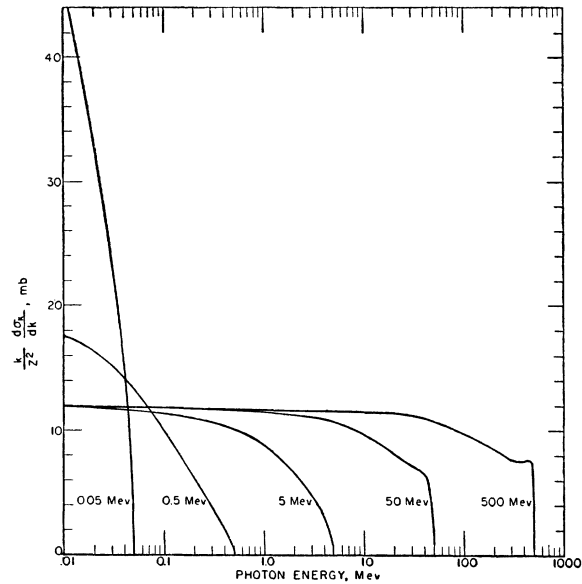


FIG. 3. Dependence of the Born-approximation cross section integrated over the photon directions on the photon and electron energy. The ordinate values for these curves are obtained from Formula 3BN for 0.05- and 0.50-Mev electrons, and from Formula 3BS (e) for 5-, 50-, and 500-Mev electrons.

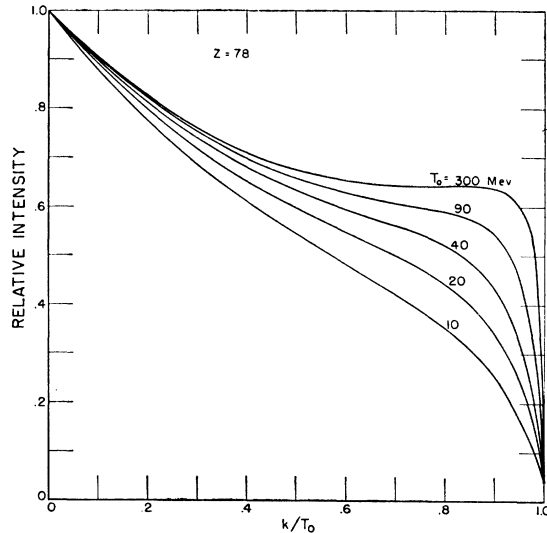


FIG. 4. Dependence of the bremsstrahlung spectrum shape on the electron kinetic energy for a platinum target ( $Z=78$ ). The relative intensity (defined as proportional to the product of the photon energy and number per unit time) is integrated over the photon direction and is normalized to unity for zero photon energies. The intensity values were computed from Formula 3BS(e).

better than 2% for electron kinetic energies above 50 Mev and for  $Z$  equal to 80.

D. Graphical Representations of the Formulas

A general picture of the dependence of the cross-section formulas in Sec. IIC on the electron and photon

TABLE II. Bremsstrahlung cross-section formulas with Coulomb correction.

**Formula 1CS**—Differential in photon energy and in photon and electron emission angles.  
Approximation (J), (N). Reference formula (7b.13) in reference (m).

$$d\sigma_{k,\theta_0,\theta,\phi} = \frac{Z^2}{137} \left(\frac{r_0}{2\pi}\right)^2 \frac{dk}{k} \frac{p}{p_0} \frac{d\Omega_e d\Omega_p}{q_1^2} \left| \int_{q_x}^{\infty} dy \frac{(y^2 - q_x^2)^{\frac{1}{2}} (1 - F(y))}{y} \int_0^{\infty} d\rho \cdot \rho J_1(q_1 \rho) J_1[\rho (y^2 - q_x^2)^{\frac{1}{2}}] \exp \left\{ 2ia \int_0^{\infty} \frac{J_0(x\rho) [1 - F(x)] dx}{x} \right\} \right|^2$$

$$\times \left\{ \frac{p^2 \sin^2 \theta}{(E - \cos \theta)^2} (4E_0^2 - q^2) + \frac{p_0^2 \sin^2 \theta_0}{(E_0 - p_0 \cos \theta_0)^2} (4E^2 - q^2) - \frac{2p p_0 \sin \theta \sin \theta_0 \cos \phi (4EE_0 - q^2) + 2k^2 (p^2 \sin^2 \theta + p_0^2 \sin^2 \theta_0 - 2p p_0 \sin \theta \sin \theta_0 \cos \phi)}{(E - p \cos \theta) (E_0 - p_0 \cos \theta_0)} \right\},$$

where

$$q^2 = p^2 + p_0^2 + k^2 - 2p_0 k \cos \theta_0 + 2pk \cos \theta - 2p_0 p (\cos \theta \cos \theta_0 + \sin \theta \sin \theta_0 \cos \phi)$$

$$q_x = p_0 \cos \theta_0 + p \cos \theta - k; \quad q_1^2 = p_0^2 \sin^2 \theta_0 + p^2 \sin^2 \theta - 2p_0 p \sin \theta_0 \sin \theta \cos \phi.$$

$F(x)$ ,  $F(y)$  are atomic form factors discussed in Sec. IIE(3) and functions of the momentum variables  $x$  and  $y$ .  
 $F(x)$  cannot be set identically to zero as discussed in reference (n).

**Formula 2CS**—Differential in photon energy and angle.  
Approximation (J), (N). Reference formula (7.2) in reference (n).

$$d\sigma_{k,\theta_0} = \frac{2Z^2 r_0^2}{137} \frac{dk}{k} \frac{d\xi}{E_0^2} \{ (E_0^2 + E^2) (3 + 2\Gamma) - 2E_0 E (1 + 4u^2 \xi^2 \Gamma) \},$$

where

$$\xi = \frac{1}{1 + u^2}; \quad u = p_0 \theta_0; \quad \Gamma = \ln \left( \frac{1}{\delta} \right) - 2 - f(Z) + \mathfrak{F} \left( \frac{\delta}{\xi} \right)$$

$$\mathfrak{F} \left( \frac{\delta}{\xi} \right) = \int_{\delta/\xi}^{\infty} \{ [1 - F(q)]^2 - 1 \} \frac{[q^2 - (\delta^2/\xi^2)]}{q^3} dq; \quad \delta = \frac{k}{2E_0 E}.$$

**Formula 2CS(a)**—Complete screening ( $\frac{\gamma}{\xi} = 0$ , where  $\gamma = \frac{100k}{E_0 E Z^{\frac{1}{2}}}$ ).

Formula 2CS with  $\mathfrak{F} = \ln \left( \frac{111\gamma}{200\xi} \right)$  or  $\Gamma = \ln \left( \frac{111Z^{-\frac{1}{2}}}{\xi} \right) - 2 - f(Z)$ ,

where

$$f(Z) = 1.2021 (Z/137)^2 \text{ for low } Z$$

$$= 0.925 (Z/137)^2 \text{ for high } Z. \text{ See reference (k) for further discussion.}$$

**Formula 2CS(b)**—Arbitrary screening.  
Formula 2CS with the form factor,  $F(q)$ , as an arbitrary function.

**Formula 2CS(c)**—Intermediate screening.  
Formula 2CS with  $\mathfrak{F}(\delta/\xi)$  given by

$\frac{6Z^{\frac{1}{2}}\xi}{121\delta}$	0.5	1.0	2.0	4.0	8.0	15.0	20.0	25.0	30.0	35.0	40.0	45.0	50.0	60.0	70.0	80.0	90.0	100.0	120.0
$-\mathfrak{F}(\delta/\xi)$	0.0145	0.0490	0.1400	0.3312	0.6758	1.126	1.367	1.564	1.731	1.875	2.001	2.114	2.216	2.393	2.545	2.676	2.793	2.897	3.078

**Formula 2CN**—Nonscreened case.  
Formula 2CS with  $\Gamma = \ln(1/\delta) - 2 - f(Z)$

**Formula 3CS**—Differential in photon energy.  
Approximation (J). Reference Formula (1) in reference (l).

$$d\sigma_k = \frac{4Z^2 r_0^2}{137} \frac{dk}{k} \left\{ \left( 1 + \left( \frac{E}{E_0} \right)^2 \right) \left[ \frac{\phi_1(\gamma)}{4} - \frac{1}{2} \ln Z - f(Z) \right] - \left( \frac{2E}{3E_0} \right) \left[ \frac{\phi_2(\gamma)}{4} - \frac{1}{2} \ln Z - f(Z) \right] \right\}.$$

**Formula 3CS(a)**—Complete screening ( $\gamma = 0$  or  $\phi_1(\gamma = 0) = 4 \ln 183$ ,  $\phi_2(\gamma = 0) = \phi_1(\gamma = 0) - \frac{2}{3}$ ).  
Formula 3CS with  $\gamma = 0$ .

$$d\sigma_k = \frac{4Z^2 r_0^2}{137} \frac{dk}{k} \left\{ \left[ 1 + \left( \frac{E}{E_0} \right)^2 - \frac{2E}{3E_0} \right] [\ln(183Z^{-\frac{1}{2}}) - f(Z)] + \frac{1E}{9E_0} \right\}.$$

**Formula 3CS(b)**—Arbitrary screening.

$$d\sigma_k = \frac{4Z^2 r_0^2}{137} \frac{dk}{k} \left\{ \left( 1 + \left( \frac{E}{E_0} \right)^2 \right) \left[ \int_{\delta}^1 (q - \delta)^2 (1 - F(q))^2 \frac{dq}{q^3} + 1 - f(Z) \right] - \frac{2E}{3E_0} E \left[ \int_{\delta}^1 \left( q^2 - 6\delta^2 q \ln \frac{q}{\delta} + 3\delta^2 q - 4\delta^3 \right) (1 - F(q))^2 \frac{dq}{q^4} + \frac{1}{9} - f(Z) \right] \right\},$$

where

$$\delta = k / (2E_0 E).$$

TABLE II.—(Continued).

**Formula 3CS(c)**—Intermediate screening I ( $\gamma < 2$ ).  
Formula 3CS with  $\phi_1(\gamma)$  and  $\phi_2(\gamma)$  given in Fig. 1.

**Formula 3CS(d)**—Intermediate screening II ( $2 < \gamma < 15$ ).  
Formula 3CS with  $\phi_1(\gamma) = \phi_2(\gamma) = 19.19 - 4 \ln \gamma - 4c(\gamma)$  with  $c(\gamma)$  given in Fig. 2.

$$d\sigma_k = \frac{4Z^2 r_0^2}{137} \frac{dk}{k} \left[ 1 + \left( \frac{E}{E_0} \right)^2 - \frac{2E}{3E_0} \right] \left[ \ln \frac{2E_0 E}{k} - \frac{1}{2} - c(\gamma) - f(Z) \right].$$

**Formula 3CN**—Nonscreened case ( $\gamma = \infty$  or  $c(\gamma) = 0$ ).  
Formula 3CS with  $\gamma = \infty$ .

$$d\sigma_k = \frac{4Z^2 r_0^2}{137} \frac{dk}{k} \left[ 1 + \left( \frac{E}{E_0} \right)^2 - \frac{2E}{3E_0} \right] \left[ \ln \frac{2E_0 E}{k} - \frac{1}{2} - f(Z) \right].$$

**Formula 4CS**—Total radiation cross section.  
Approximation (J). Reference formula (45) in reference (k).

$$\phi_{\text{rad}} = \frac{4Z^2 r_0^2}{137} \left[ \ln(183Z^{-1}) + \frac{1}{18} - f(Z) \right].$$

**Formula 4CN**—Total radiation cross section.  
Approximation (J). Reference formula (44) in reference (k).

$$\phi_{\text{rad}} = \frac{4Z^2 r_0^2}{137} \left[ \ln 2E_0 - \frac{1}{2} - f(Z) \right]$$

energies, the photon emission angle, and screening corrections is presented in Figs. 3–10. These graphs provide various types of theoretical intercomparisons primarily for energies above 1 Mev. Such a detailed examination of the predictions is useful only for the high-energy region where the theories are reasonably accurate and require much smaller corrections than in the low-energy region. The high-energy intercomparisons rely heavily on the extreme-relativistic predictions of Schiff<sup>14</sup> which depend on the validity of the complete screening approximation [see Sec. IIE (3)]. The Schiff formulas are given in a relatively simple analytical form, and have been used extensively for estimating the spectrum shape from a high-energy accelerator even though other more complicated formulas with intermediate-screening approximations are believed to be more accurate (see Table V).

(1) *Dependence of the Bremsstrahlung Spectrum on Electron Energy*

Figure 3 shows the dependence of the bremsstrahlung spectrum (integrated over the photon directions) on various initial electron kinetic energies for a platinum target ( $Z=78$ ). The spectra for 0.05- and 0.5-Mev electrons were calculated from Formula 3BN. The spectra for 5-, 50-, and 500-Mev electrons were calculated from Formula 3BS(e). Figure 4 compares spectrum shapes predicted by Formula 3BS(e) for various electron energies.

(2) *Dependence of the Bremsstrahlung Spectrum on Photon Angle*

Figures 5(a)–(e) show the dependence of the spectrum shape on the reduced photon angle,  $E_0\theta_0$ , as ob-

tained from Formula 2BS. The figures show that as the emission angle increases, the relative number of high-frequency photons increases until the trend reverses at the larger angles. For comparison, the spectrum shape integrated over the emission angle is evaluated from

TABLE III. Approximations, conditions of validity, and references for bremsstrahlung formulas of Tables I and II.

Approximation	Condition of validity
A. Nonscreened	$60Z^{-1}(1+p_0^2\theta_0^2) \gg (E_0E/k)$
B. Nonscreened	$137Z^{-1} \gg (E_0E/k)$
C. Nonscreened	$E_0 \ll 137Z^{-1}$
D. Complete screening	$60Z^{-1}(1+p_0^2\theta_0^2) \ll (E_0E/k)$
E. Complete screening	$137Z^{-1} \gg (E_0E/k)$
F. Complete screening	$E_0 \gg 137Z^{-1}$
G. Approximate screening potential:	$(Ze/r) \exp(-r/a)$
H. Born approximation	$(2\pi Z/137\beta_0), (2\pi Z/137\beta) \ll 1$
I. Nonrelativistic	$\beta_0 \ll 1$
J. Extreme relativistic	$E_0, E, k \gg 1$
K. Small angles	$\sin\theta = \theta$
L. Large angles	$\theta_0 \gg 0$
M. Approximation in electron angle integration. Result not accurate for	$\theta_0 \lesssim (Z^{1/2}/111E_0)$
N. Small angles	$\frac{1}{2} < p_0\theta_0 < 5$

<sup>a</sup> H. Bethe and W. Heitler, Proc. Roy. Soc. (London) **A146**, 83 (1934).  
<sup>b</sup> H. Bethe, Proc. Cambridge Phil. Soc. **30**, 524 (1933).  
<sup>c</sup> W. Heitler, *Quantum Theory of Radiation* (Oxford University Press, London, 1954), third edition, p. 244.  
<sup>d</sup> F. Sauter, Ann. Physik **20**, 404 (1934).  
<sup>e</sup> G. Racah, Nuovo cimento **11**, 469 (1934).  
<sup>f</sup> R. L. Gluckstern and M. H. Hull, Jr., Phys. Rev. **90**, 1030 (1953).  
<sup>g</sup> A. Sommerfeld, *Wellenmechanik* (Frederick Ungar, New York, 1950), Chap. 7.  
<sup>h</sup> L. I. Schiff, Phys. Rev. **83**, 252 (1951).  
<sup>i</sup> P. V. C. Hough, Phys. Rev. **74**, 80 (1948).  
<sup>j</sup> E. Segre, *Experimental Nuclear Physics* (John Wiley & Sons, Inc., New York, 1953), p. 260.  
<sup>k</sup> Davies, Bethe, and Maximon, Phys. Rev. **93**, 788 (1954).  
<sup>l</sup> H. Olsen, Phys. Rev. **99**, 1335 (1955).  
<sup>m</sup> Olsen, Maximon, and Wergeland, Phys. Rev. **106**, 27 (1957).  
<sup>n</sup> H. Olsen and L. C. Maximon, Phys. Rev. **114**, 887 (1959).

<sup>14</sup> L. I. Schiff, Phys. Rev. **83**, 252 (1951).

Formula 3BS(e) and is shown by the dashed line. In Figs. 6(a)-(e), the dependence of the cross section (Formula 2BS) on the photon emission angle,  $\theta_0$ , is plotted for various photon and electron energies.

The spectrum shape integrated<sup>15</sup> over the photon directions with the limits from zero to a maximum value of  $\theta_0$  equal to  $\Theta$  is of practical interest to experi-

mentalists. Figures 7(a)-(e) show the spectra obtained for different values of  $E_0\Theta$  by integrating Formula 2BS within the above limits of  $\theta_0$ . These curves facilitate estimates of the change in thin-target spectra for different experimental arrangements that subtend various angles. In Figs. 8(a)-(c), the curves give estimates of the fraction of the total number of photons at any

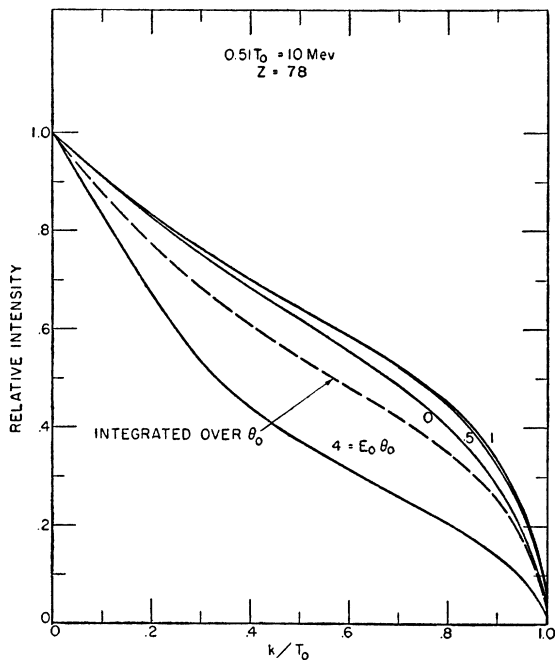


FIG. 5(a)

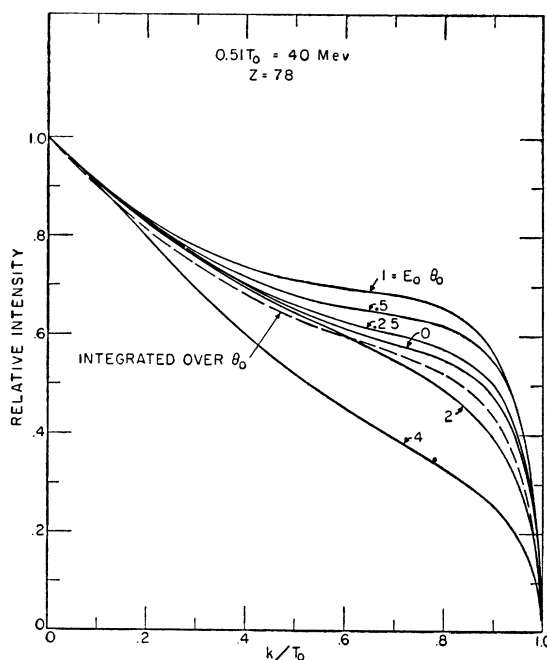


FIG. 5(c)

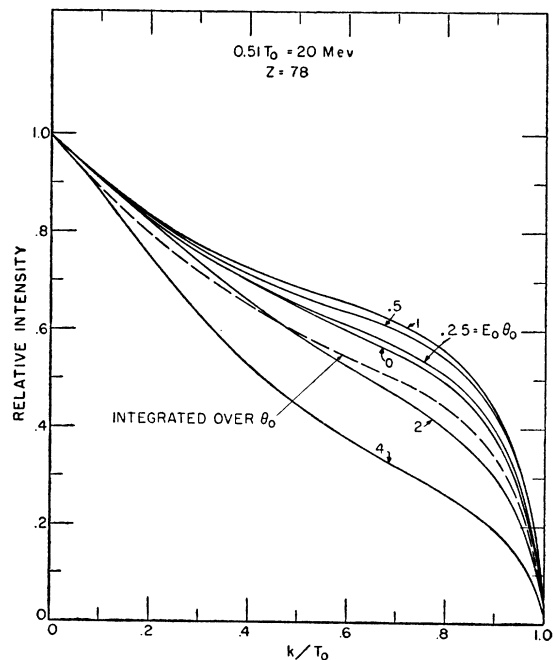


FIG. 5(b)

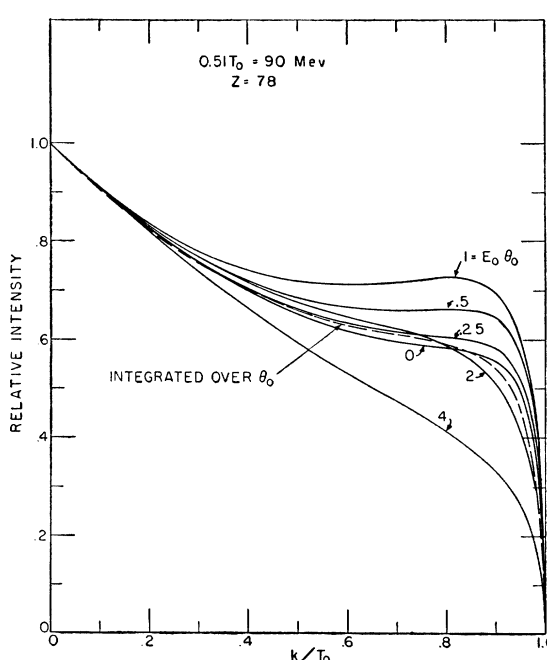


FIG. 5(d)

<sup>15</sup> J. H. Hubbell, J. Appl. Phys. 30, 981 (1959).

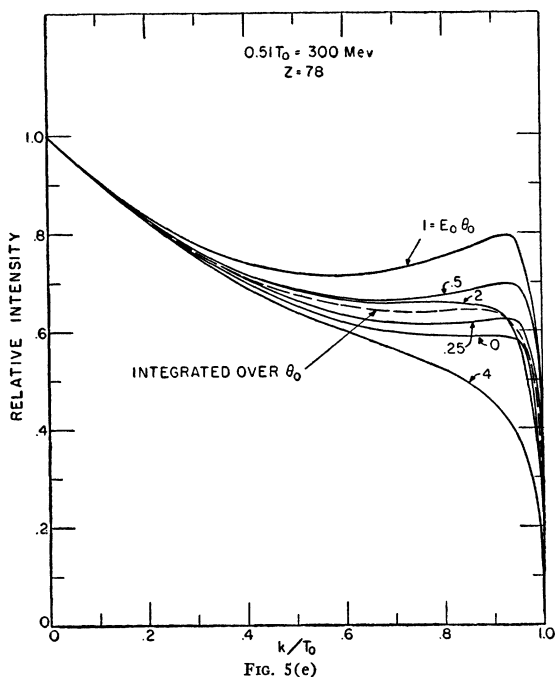


FIG. 5(e)

FIG. 5(a) Dependence of the Schiff spectrum shape on the photon emission angle,  $\theta_0$ , for 10-Mev electrons and for  $Z=78$ . The data are obtained from Formula 2BS (solid lines) and from Formula 3BS(e) (dashed line). The values for the intensities (defined as proportional to the product of the photon energy and number per unit time) are normalized to unity at the zero photon energy. (b) Dependence of the Schiff spectrum shape on the photon emission angle,  $\theta_0$ , for 20-Mev electrons and for  $Z=78$ . (c) Dependence of the Schiff spectrum shape on the photon emission angle,  $\theta_0$ , for 40-Mev electrons and for  $Z=78$ . (d) Dependence of the Schiff spectrum shape on the photon emission angle,  $\theta_0$ , for 90-Mev electrons and for  $Z=78$ . (e) Dependence of the Schiff spectrum shape on the photon emission angle,  $\theta_0$ , for 300-Mev electrons.

given energy that are included within the angular limits from zero to  $E_0\Theta$ ; these curves are obtained by graphical integration from Figs. 6(a), (c), and (e) for initial electron kinetic energies of 10, 40, and 300 Mev.

Figures 5–8 present some predictions of the Born-approximation formulas given in Table I. For comparison, the spectrum shapes as a function of the photon emission angle that are predicted by the more accurate extreme-relativistic Formula 2CS(c) in Table II, are shown in Figs. 9(a) through (e) with a normalization of unity for zero photon energy. The spectra for electron kinetic energies of 10, 20, and 40 Mev, Figs. 9(a), (b), and (c), are predicted with a zero Coulomb correction factor,  $f(Z)=0$ , in Formula 2CS(c), and the spectra for electron kinetic energies of 90 and 300 Mev, Figs. 9(d) and (e), include the Coulomb correction factor for  $Z=78$ . A comparison of the spectral shapes with and without the Coulomb correction factor shows only small differences compared to the larger effects that occur with different types of screening approximations.

### (3) Screening Effects and Coulomb Corrections

Figures 10(a)–(e) intercompare Formula 2BS ( $0^\circ$  Schiff), Formula 3BS(c) (Schiff's formula integrated

over the photon angle), Formula 3BS (Bethe-Heitler's formula integrated over the photon angle), and the latter formula including the Davies, Bethe, Maximon correction [Formula 3CS and Sec. IIE(1)]. The three curves that are integrated over photon angle are appreciably different in shape. For example, the curves labeled "Schiff" and "Davies, Bethe, Maximon" are 10% different for an electron energy of 10 Mev at a fractional photon energy of 0.7 with the normalization used in this figure. For the sake of completeness, the spectra corrected for multiple scattering are also plotted in these figures. The multiple scattering correction as calculated by Hisdal<sup>16</sup> is discussed in Sec. IV.

## E. Corrections for the Cross-Section Formulas

Various corrections have been obtained for the formulas given in Sec. IIC. These corrections may be classified according to three types: (1) Coulomb corrections, (2) high-frequency-limit corrections, and (3) screening corrections. In each case, the correction is restricted to a particular energy region, and is intended to apply only to the formula for a particular differential form of cross section as specified below.

### (1) Coulomb Corrections

(a) *Nonrelativistic energies.*—In the nonrelativistic region where  $T_0 \ll 1$ , Elwert<sup>17</sup> has estimated a multiplicative Coulomb correction factor for the cross-section Formula 3BN(a). The Elwert factor,  $f_E$ , can be written as

$$f_E = \frac{\beta_0 \{1 - \exp[-(2\pi Z/137\beta_0)]\}}{\beta \{1 - \exp[-(2\pi Z/137\beta)]\}}. \quad (\text{II-6})$$

This factor is valid only if  $(Z/137)(\beta^{-1} - \beta_0^{-1}) \ll 1$ . This requirement forbids the use of the Elwert factor near the high-frequency limit. In addition, the Elwert correction was derived on the basis of a comparison between the nonrelativistic Born-approximation and the nonrelativistic Sommerfeld calculations. Therefore the factor is restricted to nonrelativistic electron energies. For higher electron energies (of the order of the electron rest energy), the experimental results in Sec. IIF show that the Elwert factor breaks down. As a rough guide, the Elwert factor may be expected to give results that are accurate to about 10% for electron energies below about 0.1 Mev.

(b) *Intermediate energies.*—In the energy region from roughly 0.1 to 2.0 Mev, Coulomb corrections to the Born-approximation formulas are not available in analytical form. Therefore these corrections must be estimated empirically from experimental results (Sec. IIF). For the cross-section formulas differential in photon energy,  $d\sigma_k$ , such empirical corrections cannot

<sup>16</sup> E. Hisdal, Phys. Rev. **105**, 1821 (1957).

<sup>17</sup> G. Elwert, Ann. Physik **34**, 178 (1939).

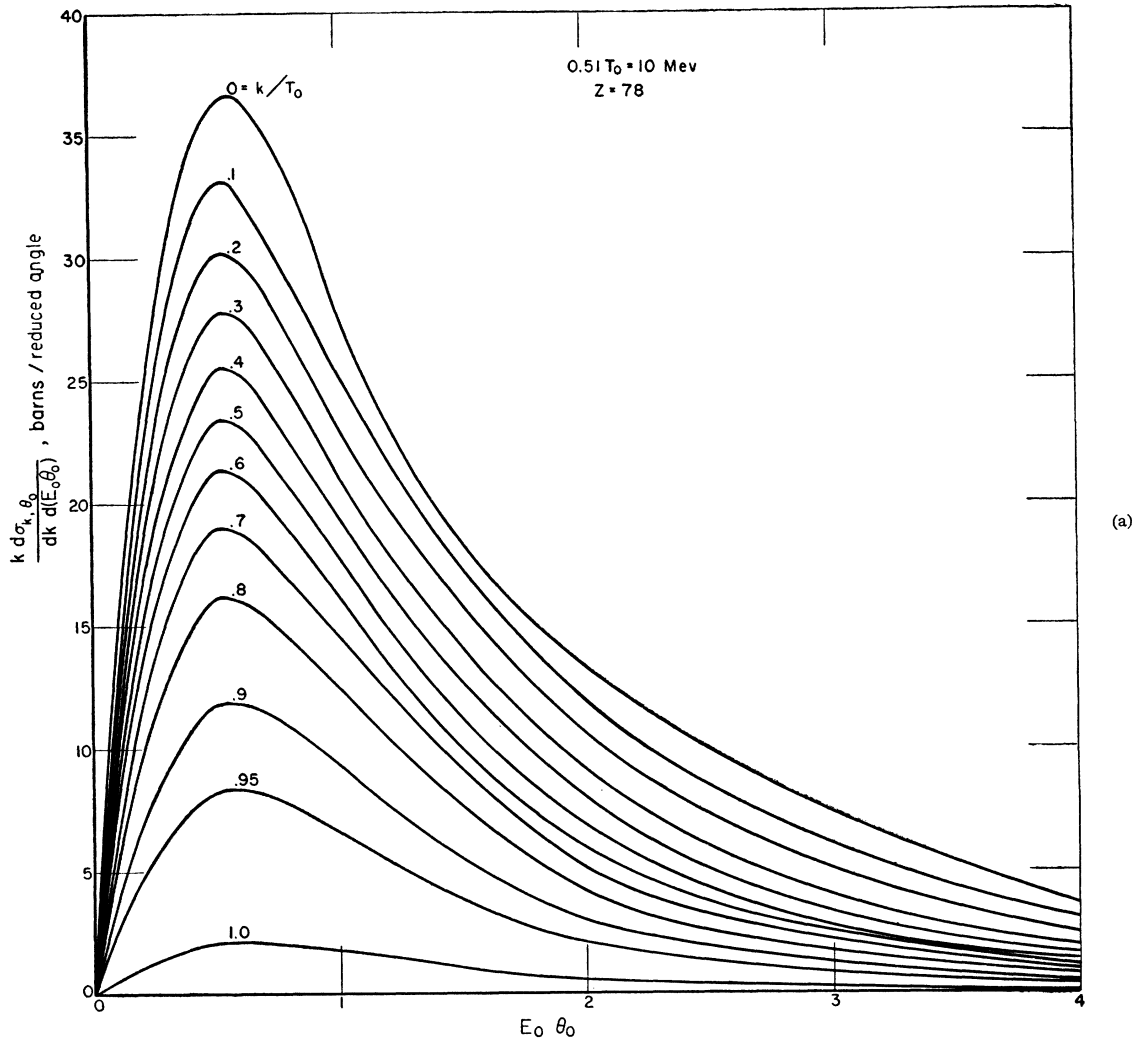


FIG. 6. Angular dependence of the Schiff cross section (Formula 2BS,  $Z=78$ ) at various photon energies for the following electron energies: (a) 10 Mev, (b) 20 Mev, (c) 40 Mev, (d) 90 Mev, and (e) 300 Mev.

(Figs. 6(b) to 6(e) continued on following pages)

be determined in enough detail from the available data to cover the whole energy region. However, corrected estimates of the integrated cross section,  $\phi_{rad}$ , are given in Sec. IIF from which empirical correction factors can be obtained. The results indicate that the corrections to the Born-approximation formulas for  $\phi_{rad}$  are as large as a factor of two in the energy region close to the electron rest energy, and less than 10% in the energy region from about 4 to 20 Mev.

(c) *Extreme-relativistic energies.*—In this energy region, formulas that include the Coulomb correction for the differential cross sections  $d\sigma_{k,\theta_0,\phi}$  and  $d\sigma_k$  are given in Table II. A comparison of the formulas in Tables I and II shows that the Coulomb correction can be applied to the Born-approximation formulas for  $d\sigma_k$  by

the addition of

$$\Delta = -\frac{4Z^2 r_0^2}{137} \frac{dk}{k} \left[ 1 + \left( \frac{E}{E_0} \right)^2 - \frac{2E}{3E_0} \right] f(Z), \quad (II-7)$$

where  $f(Z)$  is approximately equal<sup>13</sup> to  $1.20(Z/137)^2$  for low  $Z$  and  $0.925(Z/137)^2$  for high  $Z$ . This additive term is independent of the type of screening approximation that is used and is similar to the correction derived for the pair production process.<sup>11</sup> For lead and energies above 50 Mev, the correction decreases the Born-approximation  $\phi_{rad}$  with intermediate screening by about 10%. The corrected cross section should be accurate to about 2%.

Accurate experimental data corroborating the cross-section values predicted by these formulas are not yet

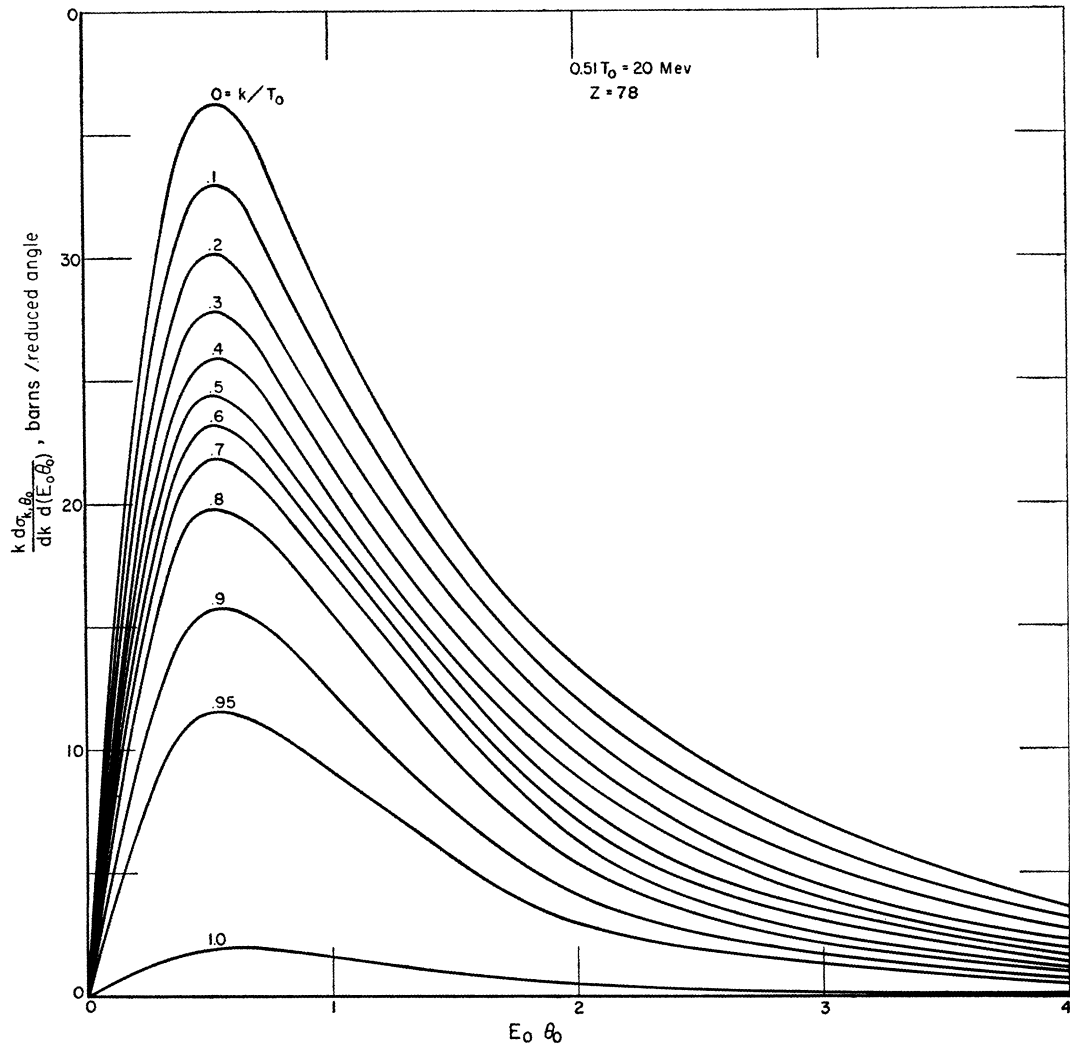


FIG. 6(b)

available. However, confirmation is available in the results of absolute pair cross sections. The ratios of the experimental pair-production cross sections to the Born-approximation cross sections are found to agree with the Davies, Bethe, Maximon<sup>13</sup> values, as shown in Fig. 11.

(2) High-Frequency-Limit Corrections

The formulas in Tables I and II are derived on the basis of certain approximations which do not permit an evaluation of the cross section at the high-frequency limit. This shortcoming has been emphasized by various experimental studies<sup>18</sup> which indicate that the cross section has a finite value at this limit.

Recent calculations made in the Sauter approximation (expansion in powers of  $Z/137\beta_0$  and  $Z/137$ ) by Fano<sup>19</sup> predict a finite value for the cross section at the

high-frequency limit. In contrast, the cross section with the Born-approximation (expansion in powers of  $Z/137\beta_0$  and  $Z/137\beta$ ) becomes zero at the limit. The cross-section formulas for the high-frequency limit obtained by Fano are<sup>20</sup>

$$[d\sigma_{k,\theta_0}]_{k=\tau_0} = \frac{Z^2 r_0^2 \beta_0}{137^2 k^2 E_0^3} \frac{dk}{k} \frac{4\pi \sin^3 \theta_0 d\theta_0}{(1 - \beta_0 \cos \theta_0)^4} \times \left\{ 1 + \frac{1}{2} E_0 (E_0 - 1) (E_0 - 2) (1 - \beta_0 \cos \theta_0) \right\} \quad (\text{II-8})$$

and, after integration over  $\theta_0$ ,

$$[d\sigma_k]_{k=\tau_0} = 4\pi \frac{Z^3}{137^2} \frac{dk}{k} \frac{E_0 \beta_0}{(E_0 - 1)^2} \times \left\{ \frac{4}{3} + \frac{E_0 (E_0 - 2)}{(E_0 + 1)} \left[ 1 - \frac{1}{2\beta_0 E_0^2} \ln \left( \frac{1 + \beta_0}{1 - \beta_0} \right) \right] \right\}. \quad (\text{II-9})$$

<sup>18</sup> W. C. Miller and B. Waldman, *Phys. Rev.* **75**, 425 (1949); Fuller, Hayward, and Koch, *ibid.* **109**, 630 (1958); D. Jamnik (private communication).

<sup>19</sup> U. Fano, *Phys. Rev.* (to be published).

<sup>20</sup> The cross section differential in  $\theta_0$  is proportional to  $\sin^3 \theta_0$ , therefore, both the Sauter-approximation and the Born-approximation calculations predict that the cross section at the high-frequency limit is zero for  $\theta_0$  equal to zero.

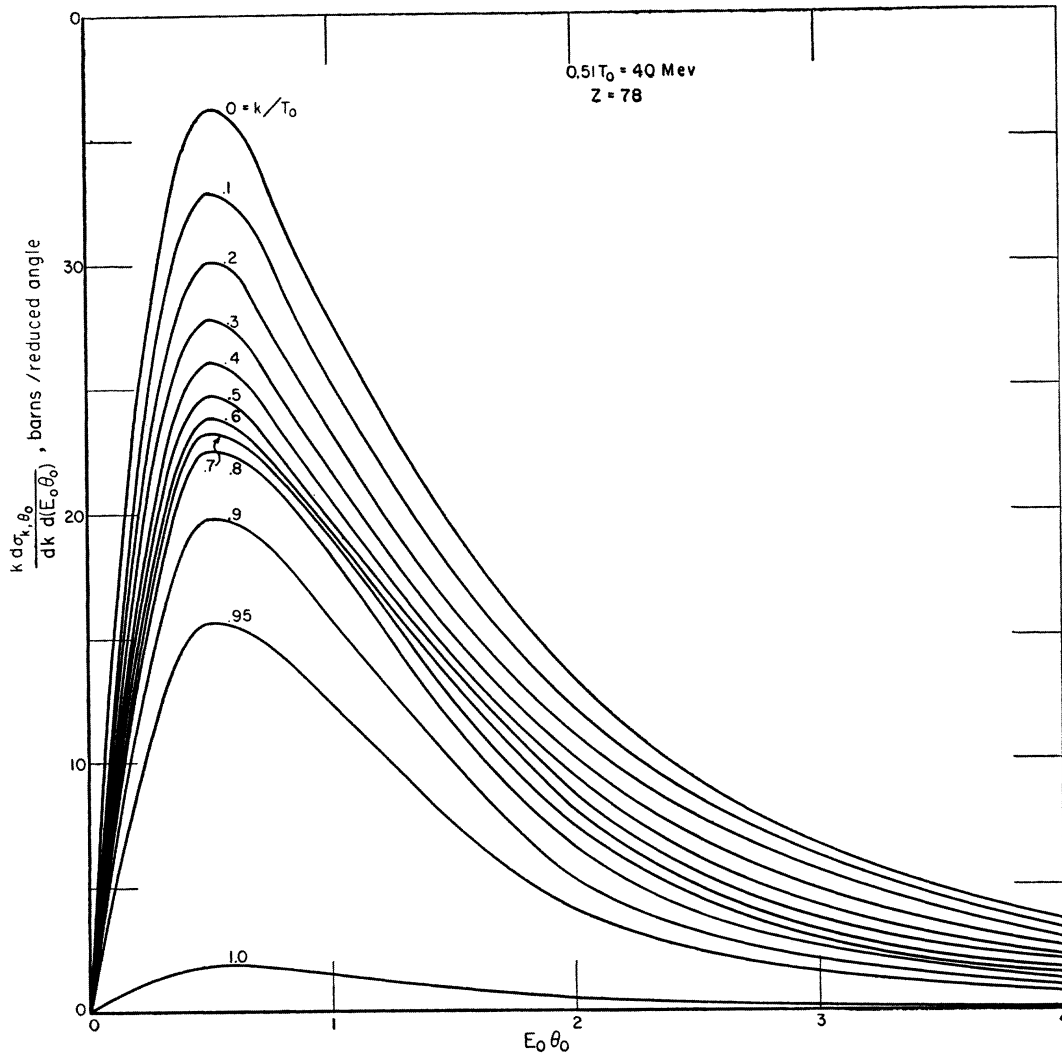


FIG. 6(c)

Fano, Koch, and Motz<sup>21</sup> have shown that Formula (II-9) overestimates the cross section at the high-frequency limit and that a more accurate estimate is obtained for a given electron kinetic energy if this formula is multiplied by the ratio of the "exact" to the Sauter photoelectric cross sections.<sup>22</sup> A summary of their results is given in Fig. 12 which shows the dependence of the bremsstrahlung cross section (integrated over photon direction) at the high-frequency limit on the incident electron energy for aluminum and gold targets. The solid lines (Sauter-Fano) are predicted by Formula (II-9) and the dashed lines (corrected Sauter-Fano) are estimated to be the corrected cross-section

values. A comparison of the theoretical and experimental values indicates that the true cross sections at the high-frequency limit are predicted by the dashed curves with an accuracy of approximately 20%.

(3) Screening Corrections

Screening effects are most important for extreme-relativistic and for nonrelativistic electron kinetic energies. Corrections for screening have been adequately included only in the extreme relativistic calculations, where  $E_0, E, k \gg 1$ . The screening corrections for both the Born-approximation and Coulomb-corrected formulas in Tables I and II have been given by the Born-approximation procedure. In these screening calculations, the cross section is proportional to the square of the matrix element

$$M = \int V(r) \exp(i\mathbf{q} \cdot \mathbf{r}) d\tau, \tag{II-10}$$

<sup>21</sup> Fano, Koch, and Motz, Phys. Rev. **112**, 1679 (1958).

<sup>22</sup> Detailed formulas for the Sauter photoelectric cross section and for the "exact" cross sections of Sauter-Stobbe and Nagasaka are given by Heitler<sup>9</sup> and by G. White Grodstein, Natl. Bur. Standards Circ. No. 583 (1957). The "exact" photoelectric cross-section formula for high energies has been calculated recently by R. H. Pratt, thesis, University of Chicago (June, 1959), and Phys. Rev. (to be published).

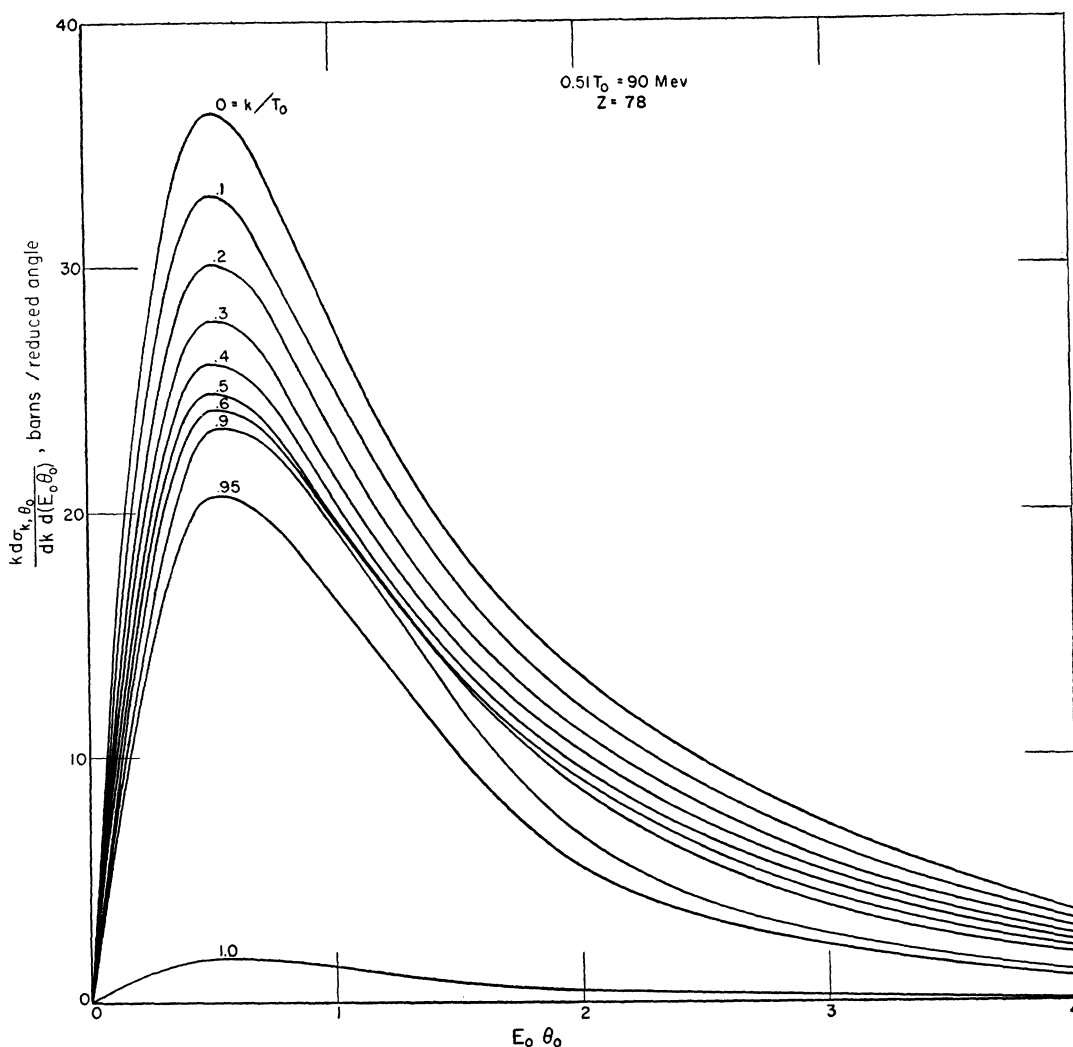


FIG. 6(d)

where  $V(r)$  is the potential that determines the interaction for the bremsstrahlung process and  $\mathbf{r}$  is the radius vector in units of the Compton wavelength,  $\lambda_0$ . This potential for an atom is represented by the sum,  $V_n + V_e$ , where  $V_n$  is the potential arising from the nuclear charge and  $V_e$  is the potential arising from the charge of the atomic electrons. If the atomic electron form factor is defined as

$$F_e(q, Z) = \frac{4\pi}{Ze} \int \rho(r) \left( \frac{\sin qr}{qr} \right) r^2 dr, \quad (\text{II-11})$$

where  $\rho(r)$  is the electron charge distribution, then the matrix element,  $M$ , can be written as proportional to the quantity  $(Z/q^2)(F_n - F_e)$ .  $F_n$  is the nuclear form factor which is roughly equal to unity.<sup>23</sup> Therefore, the unscreened differential cross-section formulas may be corrected for screening effects by including the multiplicative factor  $[1 - F_e]^2$ .

<sup>23</sup> S. J. Biel and E. H. S. Burhop, Proc. Phys. Soc. (London) **A68**, 165 (1955).

For a Thomas-Fermi model,  $F_e$  depends on the quantity  $qZ^{-1}$  where  $q$  has a minimum value of  $(p_0 - p - k)$ . At higher energies,  $q_{\min}$  becomes equal to  $(k/2E_0E)$  and screening calculations are expressed in terms of  $\gamma = 100k(E_0EZ^{\frac{1}{2}})^{-1}$ .  $\gamma$  is approximately equal to the radius of the Thomas-Fermi atom ( $r_{\text{TF}} = 137Z^{-\frac{1}{2}}$ ) divided by  $r_{\max}$ , where  $r_{\max}$  is the maximum impact parameter discussed by Heitler<sup>9</sup> and is equal to  $q_{\min}^{-1}$ . If  $r_{\max}$  is large compared to the nuclear radius but small compared to the atomic radius  $r_{\text{TF}}$ , then  $\gamma$  is large and  $F_e(q, Z) = 0$ . If  $r_{\max}$  is of the order of  $r_{\text{TF}}$ , then  $\gamma \sim 1$  and screening must be taken into account. If the impact parameter is of the order of the nuclear radius, then the distribution of the nuclear charge must be included by a nuclear form factor<sup>23</sup> although the influence of the distribution of the atomic electrons can be neglected.

The dependence of  $r_{\max}$  on the initial electron kinetic energy at all energies can be obtained by setting  $r_{\max}$  equal to  $(p_0 - p - k)^{-1}$ . The results are shown in Fig. 13 for  $k$  equal to  $0.1T_0$ ,  $0.5T_0$ , and  $0.9T_0$ . Also, the dashed

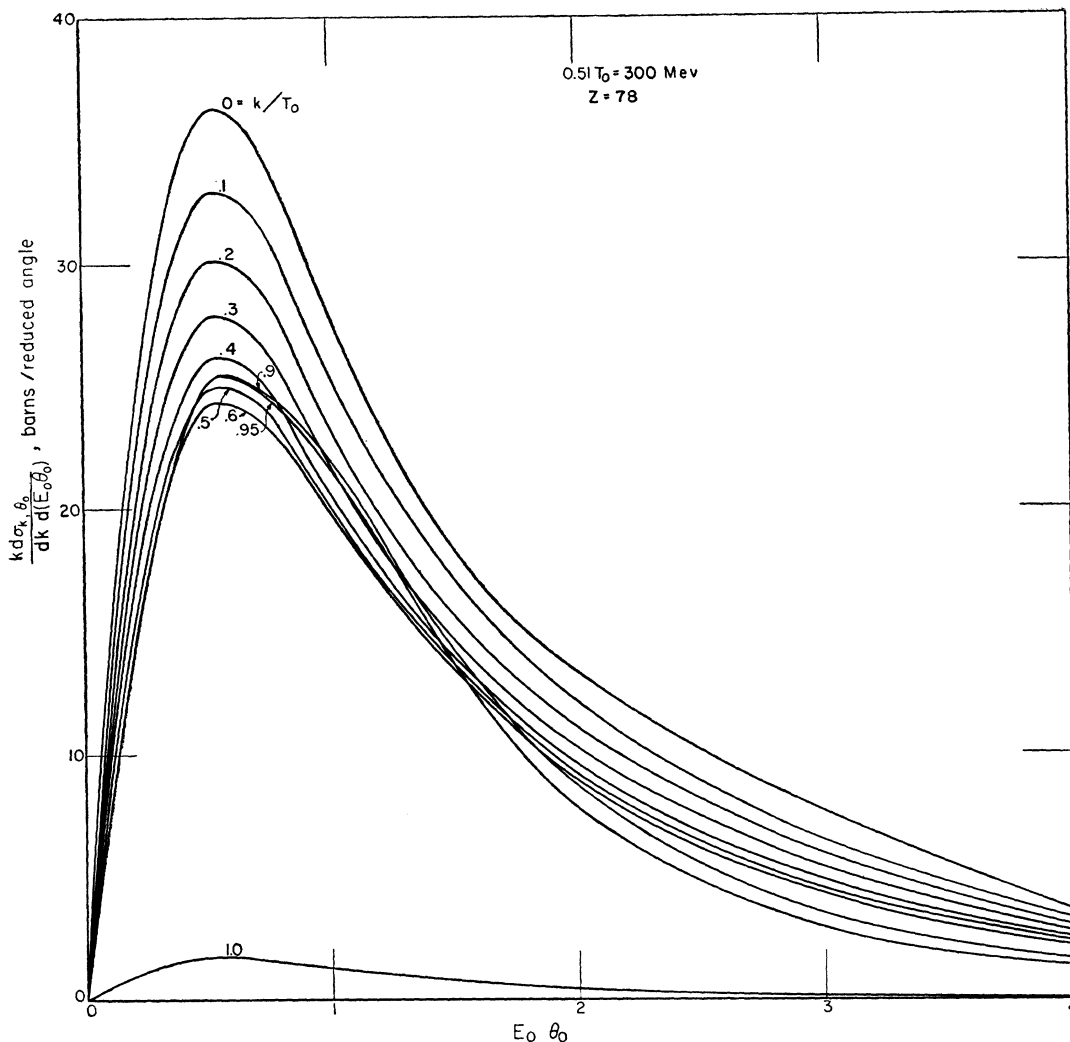


FIG. 6(e)

lines give the Thomas-Fermi atomic radii for beryllium and gold. A comparison of  $r_{\max}$  with  $r_{\text{TF}}$  shows that  $r_{\max}$  is larger than  $r_{\text{TF}}$  at low and high energies. To be specific, screening effects can be expected to become important over a large part of the spectrum for electron kinetic energies above approximately 5 Mev and below approximately 10 kev. For low fractional photon energies where  $k \leq 0.1T_0$ , screening effects are important for all values of  $T_0$ . It is interesting to observe that for the high photon energies the screening effects are the least important for values of  $T_0$  approximately equal to the electron rest energy.

The accuracy obtainable with a bremsstrahlung formula corrected for screening depends on the validity of the extreme-relativistic approximations and on the adequacy of the atomic model used to provide the form factor. Only the latter will be commented on here. The most extensive calculations and applications have been based on the Thomas-Fermi atomic model. However,

the Hartree self-consistent field model is more accurate<sup>24</sup> but more difficult to apply. The atomic form factors predicted by the two models have been compared by Nelms and Oppenheim<sup>24</sup> and are given in Fig. 14. The curves in this figure show that the accuracy of the Thomas-Fermi model decreases as the atomic number decreases.

Information concerning the influence of the form factor differences on the bremsstrahlung cross section can be obtained by referring to pair production calculations. The nuclear momentum distribution in the pair production process at extreme-relativistic energies as calculated by Jost, Luttinger, and Slotnik,<sup>25</sup> is given in Fig. 15. Their results show that the most probable  $q$  values are of the order of 0.1. Table IV gives the ratio of the Thomas-Fermi to the Hartree form factors for representative  $q$  values, as obtained by Nelms and

<sup>24</sup> A. T. Nelms and I. Oppenheim, J. Research Natl. Bur. Standards **55**, 53 (1955).

<sup>25</sup> Jost, Luttinger, and Slotnik, Phys. Rev. **80**, 189 (1950).

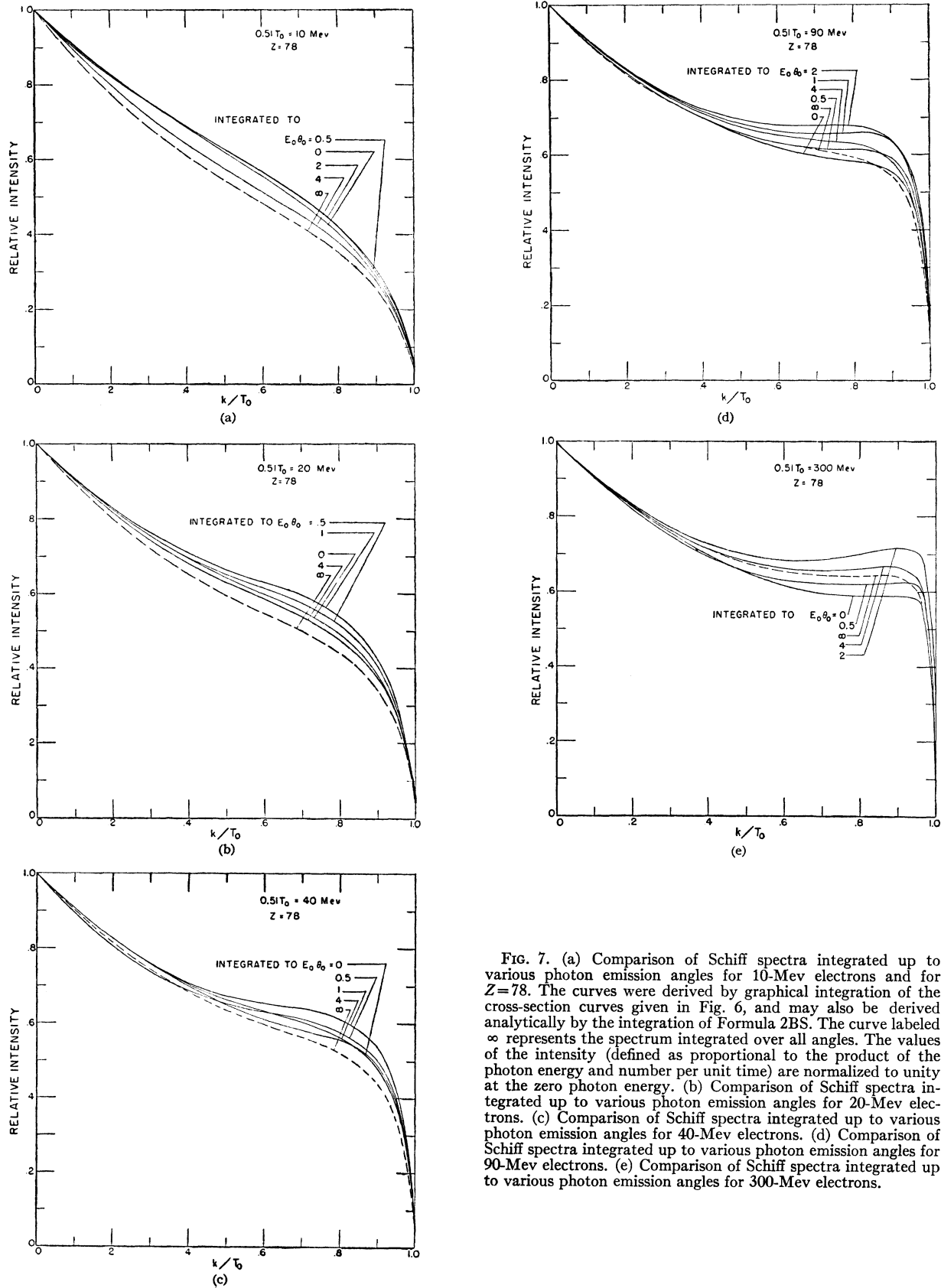


FIG. 7. (a) Comparison of Schiff spectra integrated up to various photon emission angles for 10-Mev electrons and for  $Z=78$ . The curves were derived by graphical integration of the cross-section curves given in Fig. 6, and may also be derived analytically by the integration of Formula 2BS. The curve labeled  $\infty$  represents the spectrum integrated over all angles. The values of the intensity (defined as proportional to the product of the photon energy and number per unit time) are normalized to unity at the zero photon energy. (b) Comparison of Schiff spectra integrated up to various photon emission angles for 20-Mev electrons. (c) Comparison of Schiff spectra integrated up to various photon emission angles for 40-Mev electrons. (d) Comparison of Schiff spectra integrated up to various photon emission angles for 90-Mev electrons. (e) Comparison of Schiff spectra integrated up to various photon emission angles for 300-Mev electrons.

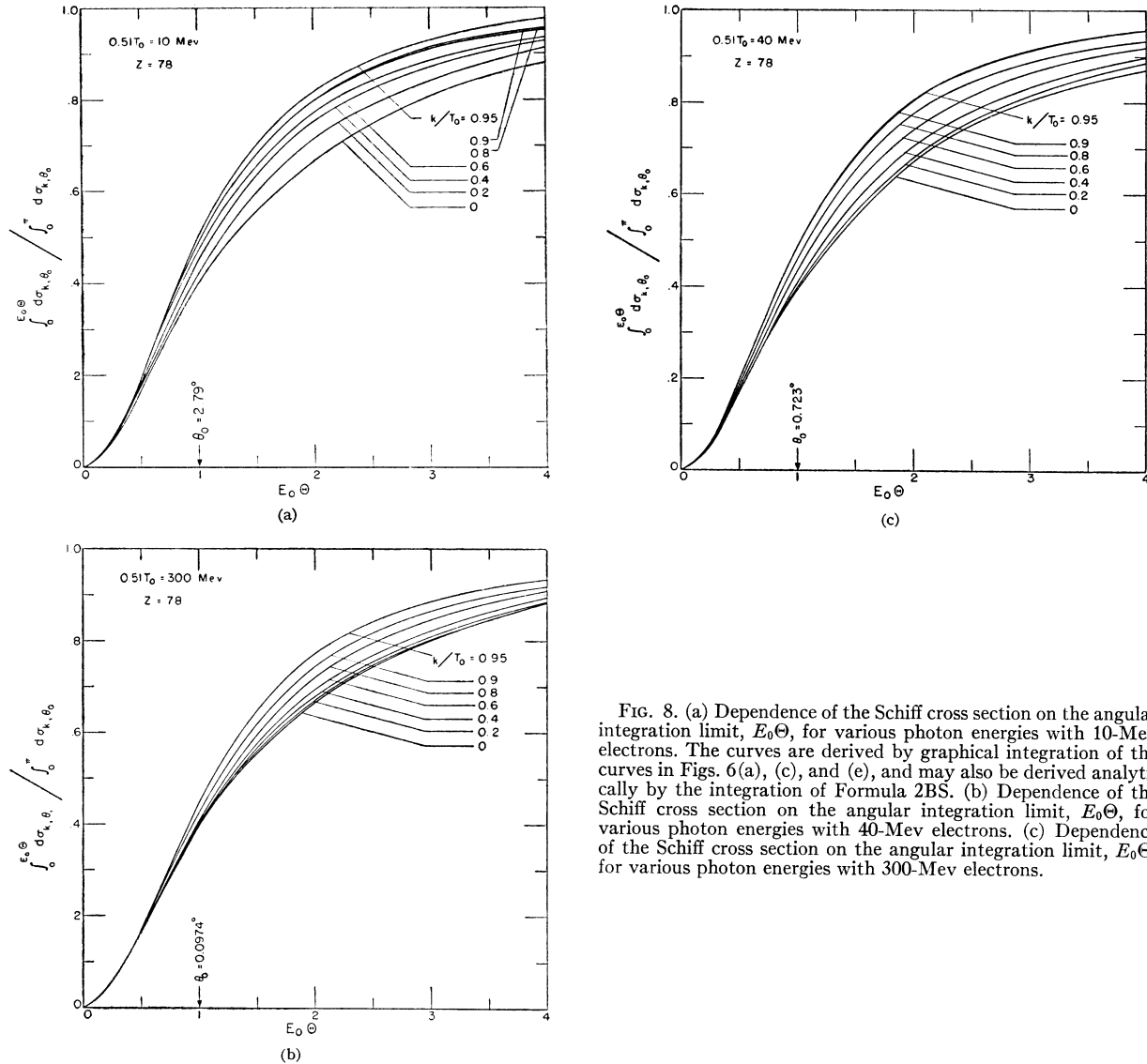


FIG. 8. (a) Dependence of the Schiff cross section on the angular integration limit,  $E_0\Theta$ , for various photon energies with 10-Mev electrons. The curves are derived by graphical integration of the curves in Figs. 6(a), (c), and (e), and may also be derived analytically by the integration of Formula 2BS. (b) Dependence of the Schiff cross section on the angular integration limit,  $E_0\Theta$ , for various photon energies with 40-Mev electrons. (c) Dependence of the Schiff cross section on the angular integration limit,  $E_0\Theta$ , for various photon energies with 300-Mev electrons.

Oppenheim<sup>24</sup> for carbon and mercury. These differences produce different estimates for the pair production cross section: for example at 60 Mev, the cross section for carbon with the Hartree form factor is increased by  $\frac{1}{2}\%$  above the cross section calculated with the Thomas-Fermi form factor.<sup>26</sup> Comparable detailed information

TABLE IV. Ratios of Thomas-Fermi to Hartree atomic form factors.

$q$	$\left(\frac{\text{Thomas-Fermi}}{\text{Hartree}}\right)_{\text{carbon}}$	$\left(\frac{\text{Thomas-Fermi}}{\text{Hartree}}\right)_{\text{mercury}}$
0.1	1.11	0.802
0.2	2.50	1.00
0.3	3.67	1.07
0.4	4.10	1.15
0.5	4.63	1.26

<sup>26</sup> R. McGinnies (private communication).

is not available for the bremsstrahlung process. However, general conclusions are possible on the basis of a comparison of the maximum impact parameters for bremsstrahlung and pair production. The maximum impact parameter for bremsstrahlung is  $(2E_0E/k)$  and the similar expression for pair production is  $(2E_+E_-/k)$  where  $E_+$  and  $E_-$  are the total energies of the positron and electron. By varying the values of  $E$  and  $k$  for fixed  $E_0$  in bremsstrahlung and the values of  $E_+$  and  $E_-$  for fixed  $k$  in pair production, we find that the important impact parameters in bremsstrahlung are larger on the average than those in pair production. This fact explains why the screening effect is much larger on  $\phi_{\text{rad}}$  than on  $\phi_{\text{pair}}$  for equal values of  $E_0$  and  $k$  (see, for example, the total cross sections for the two processes in reference 9, pp. 252 and 262). The larger screening effect indicates that the use of the Hartree form factor

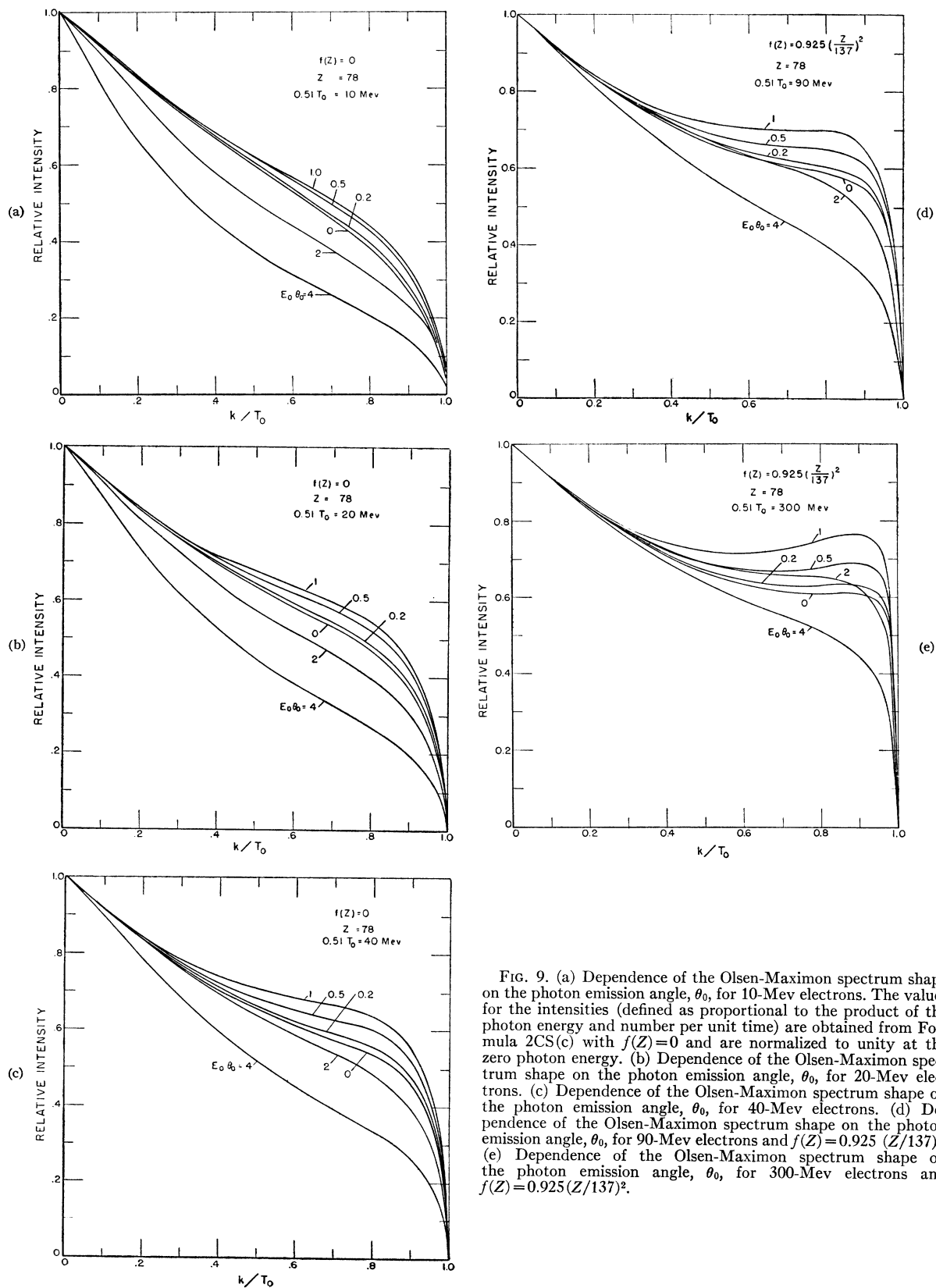


FIG. 9. (a) Dependence of the Olsen-Maximon spectrum shape on the photon emission angle,  $\theta_0$ , for 10-Mev electrons. The values for the intensities (defined as proportional to the product of the photon energy and number per unit time) are obtained from Formula 2CS(c) with  $f(Z)=0$  and are normalized to unity at the zero photon energy. (b) Dependence of the Olsen-Maximon spectrum shape on the photon emission angle,  $\theta_0$ , for 20-Mev electrons. (c) Dependence of the Olsen-Maximon spectrum shape on the photon emission angle,  $\theta_0$ , for 40-Mev electrons. (d) Dependence of the Olsen-Maximon spectrum shape on the photon emission angle,  $\theta_0$ , for 90-Mev electrons and  $f(Z)=0.925 (Z/137)^2$ . (e) Dependence of the Olsen-Maximon spectrum shape on the photon emission angle,  $\theta_0$ , for 300-Mev electrons and  $f(Z)=0.925 (Z/137)^2$ .

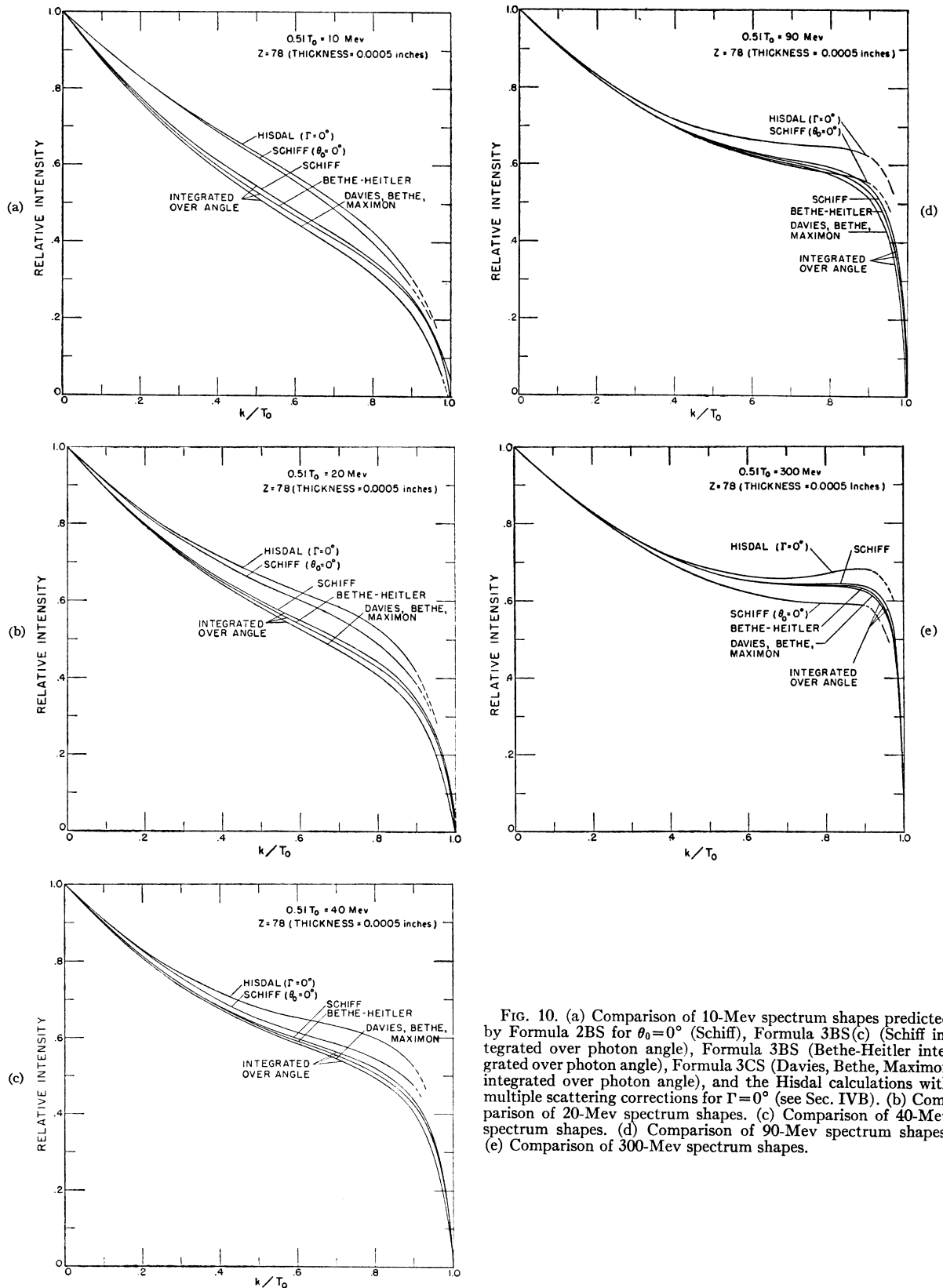


FIG. 10. (a) Comparison of 10-Mev spectrum shapes predicted by Formula 2BS for  $\theta_0=0^\circ$  (Schiff), Formula 3BS(c) (Schiff integrated over photon angle), Formula 3BS (Bethe-Heitler integrated over photon angle), Formula 3CS (Davies, Bethe, Maximon integrated over photon angle), and the Hisdal calculations with multiple scattering corrections for  $\Gamma=0^\circ$  (see Sec. IVB). (b) Comparison of 20-Mev spectrum shapes. (c) Comparison of 40-Mev spectrum shapes. (d) Comparison of 90-Mev spectrum shapes. (e) Comparison of 300-Mev spectrum shapes.

in place of the Thomas-Fermi factor will have a greater effect on  $\phi_{\text{rad}}$  than on  $\phi_{\text{pair}}$ .

The first detailed study of the influence of form factors on screened bremsstrahlung cross sections was made by Bethe.<sup>27</sup> Bethe's calculations, which are summarized in the formulas of Tables I and II, consider four types of screening:

- 1, complete screening condition:  $\gamma \approx 0$ ;
- 2, intermediate screening condition I:  $\gamma < 2$ ;
- 3, intermediate screening condition II:  $2 < \gamma < 15$ ;
- 4, no screening condition:  $\gamma \gg 1$ .

The Bethe<sup>27</sup> and Bethe-Heitler<sup>28</sup> screening calculations with intermediate conditions I and II were performed numerically using the tabulations of the atomic form factor for the Thomas-Fermi model given by Bethe.<sup>29</sup>

In the work of Schiff<sup>14</sup> analytical calculations were made possible by the use of the complete screening condition ( $\gamma \approx 0$ ) and an approximate screened atom potential,  $V$ , given by  $(Ze/r) \exp(-r/a)$ , where  $a = (111/Z^4)$ . The atomic form factor,  $F_e(q, Z)$ , corresponding to this potential is given by the quantity  $[1 + (aq)^2]^{-1}$ . For many purposes the Schiff Formulas 2BS and 3BS(e) are sufficiently accurate. Schiff<sup>14</sup> notes that compared to the intermediate screening Formula 3BS, the complete-screening Formula 3BS(e), "is larger than it should be by less than 2% for moderate values of  $Z$  and is never more than 4% high in the worst case of large  $Z$  and energies such that screening is incomplete."

A third procedure for including form factor effects was developed by Molière.<sup>30</sup> By approximating the Thomas-Fermi potential with a simple analytical expression, he obtained the following relation:

$$\frac{[1 - F_e(q, Z)]}{q^2} = \sum_{i=1}^3 \frac{\alpha_i}{\beta_i^2 + q^2}, \quad (\text{II-12})$$

where  $\alpha_1 = 0.10$ ,  $\alpha_2 = 0.55$ ,  $\alpha_3 = 0.35$ ,

$$\beta_i = Z^{\frac{1}{2}} b_i / 121; \quad b_1 = 6.0, \quad b_2 = 1.20, \quad b_3 = 0.30.$$

The Molière function has been applied by Olsen and Maximon<sup>8</sup> to obtain intermediate screening formulas that include Coulomb corrections.

The most accurate predictions of screening corrections to bremsstrahlung cross sections for specific target elements can be obtained by the use of the Hartree form factors in the formulas that permit the use of arbitrary form factors, e.g., Formulas 3BS(b) and 2CS(b). Unfortunately, the screening corrections for these formulas must be evaluated numerically and are not as convenient to use as the complete screening formulas just discussed.

<sup>27</sup> H. Bethe, Proc. Cambridge Phil. Soc. **30**, 524 (1934).

<sup>28</sup> H. Bethe and W. Heitler, Proc. Roy. Soc. (London) **A146**, 83 (1934).

<sup>29</sup> H. Bethe, Ann. Physik **5**, 385 (1930).

<sup>30</sup> G. Molière, Z. Naturforsch. **2a**, 133 (1947).

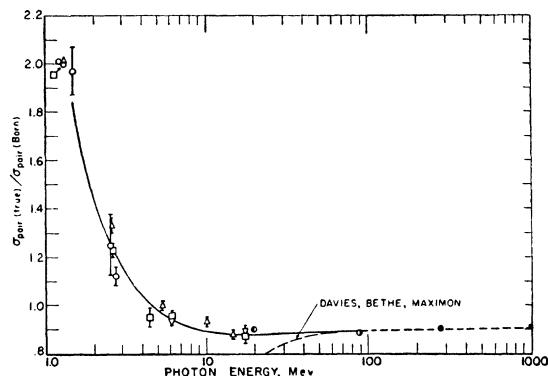


FIG. 11. Dependence of the pair cross-section ratio,  $d\sigma_{\text{pair}}(\text{true})/d\sigma_{\text{pair}}(\text{Born})$ , on the photon energy. The solid curve is taken from Grodstein<sup>22</sup> and the dashed curve is taken from reference 13.

## F. Comparison of Theory and Experiment

Very few experimental determinations of the bremsstrahlung cross section are available for comparison with the estimates given in Secs. IIC, D, and E. At present, experimental data on cross sections have been obtained for electron kinetic energies of 34 keV<sup>31</sup> by Amrehn<sup>32</sup> and Röss,<sup>32</sup> 50 keV by Motz and Placious,<sup>33</sup> 90 to 180 keV by Mausbeck<sup>34</sup> and Zeh,<sup>34</sup> 0.5 and 1.0 MeV by Motz,<sup>35</sup> and 2.72, 4.54, and 9.66 MeV by

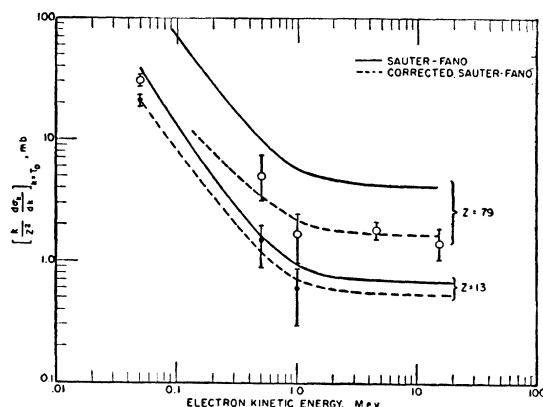


FIG. 12. Dependence of the bremsstrahlung cross section at the high-frequency limit, integrated over photon direction, on the incident electron kinetic energy. These data are obtained from reference 21, and the dashed curves are estimated to give the most accurate values for the cross section.

<sup>31</sup> Most of the experimental data that is available in this low-energy region has been produced by the pioneering work of Kulenkampff and co-workers. Their measurements give extensive information about relative angular distributions and spectra from thin targets, and show general agreement with the nonrelativistic Sommerfeld theory.<sup>9</sup> The details of their various results are not included in this report which is primarily concerned with absolute cross-section measurements and comparisons with the Born-approximation theory.

<sup>32</sup> H. Amrehn, Z. Physik **144**, 529 (1956); D. Röss, thesis, University of Würzburg (December, 1957).

<sup>33</sup> J. W. Motz and R. C. Placious, Phys. Rev. **109**, 235 (1958).

<sup>34</sup> H. Mausbeck, thesis, University of Würzburg (1957); H. Zeh, thesis, University of Würzburg (1957).

<sup>35</sup> J. W. Motz, Phys. Rev. **100**, 1560 (1955).

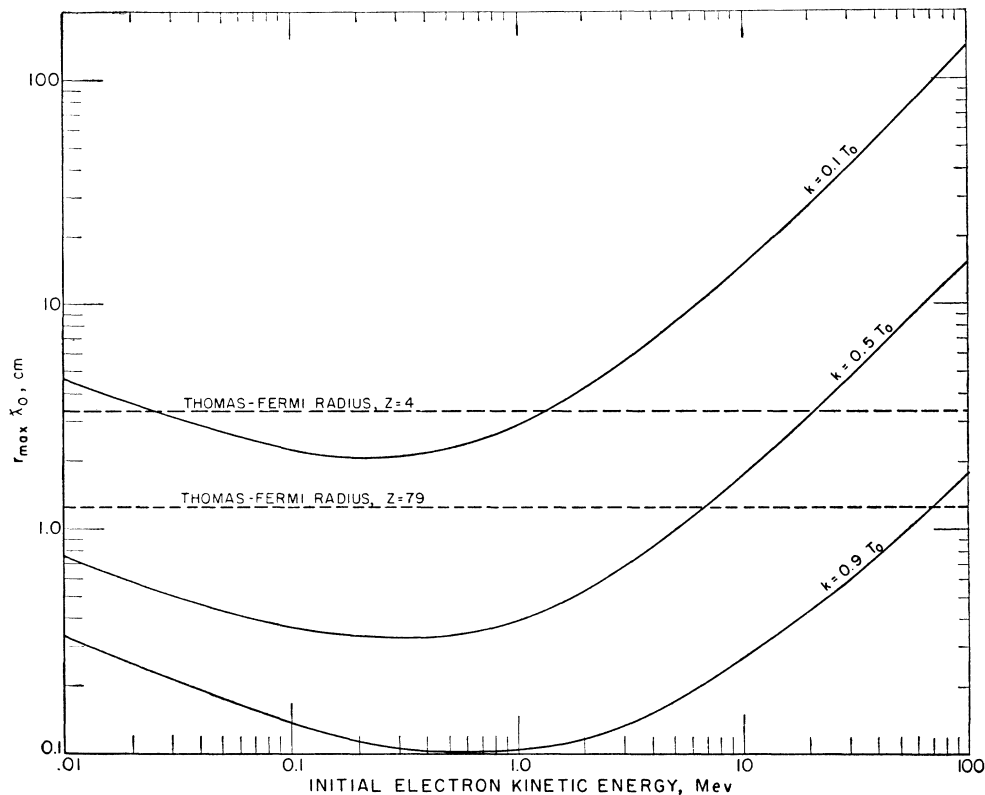


FIG. 13. Dependence of  $r_{\max}$  on the initial electron kinetic energy for  $k$  equal to  $0.1T_0$ ,  $0.5T_0$ , and  $0.9T_0$ .  $r_{\max}$  is the reciprocal of the minimum momentum transferred to the nucleus ( $=p_0 - p - k$ ), and is given in units of the Compton wavelength,  $\lambda_0$ . The dashed lines give the values of the Thomas-Fermi radius ( $=137Z^{-1}$ ) for beryllium and gold.

Starfelt and Koch.<sup>36</sup> The important results of these studies are combined and summarized below.

(1) *Cross-Section Differential in Photon Energy and Angle*

For electron kinetic energies that are small compared with the electron rest energy, the experimental results<sup>31-33</sup> show general agreement with the Sommerfeld theory<sup>5</sup> except for certain minor discrepancies which probably occur because the theory does not account for relativistic and screening effects. On the other hand, the Born-approximation theory (Formula 2BN) is seriously inadequate in this energy region and no analytical correction factors for the Born-approximation formula are available in this differential form. Furthermore, no quantitative studies are available on the importance of screening.

For electron kinetic energies that are of the same order of magnitude as the electron rest energy, the Born-approximation theory (Formula 2BN) underestimates the experimental cross section<sup>34,35</sup> as shown by the comparison in Fig. 16. These data also show that the differences between the theory and experiment increase with (a) the photon energy, (b) the photon angle, and (c) the atomic number of the target.

For electron kinetic energies that are large compared with the electron rest energy, the experimental results<sup>36</sup>

agree within 10% with the Born-approximation theory. For example, in Fig. 17, the experimental cross sections for gold at 4.54 Mev<sup>36</sup> show general agreement with the predictions of the screened, extreme-relativistic Schiff Formula 2BS and of the unscreened Sauter Formula 2BN. There are differences in detail (generally less than 10% in this energy region): (a) near the high-frequency limit, the experimental cross sections are greater than the Schiff cross sections which in turn are greater than the Sauter cross sections; (b) in the low-frequency region, the experimental cross sections show good agreement with the Schiff cross sections, but are less than the unscreened Sauter cross sections. For low  $Z$  targets, there is better agreement with the Sauter formula.

(2) *Cross-Section Differential in Photon Energy*

A comparison<sup>21</sup> of experimental and theoretical values for the cross section differential in photon energy,  $d\sigma_k$ , is given in Figs. 18-21 for electron energies of 0.05, 0.5, 1.0, and 4.5 Mev. Each of these figures gives the estimates of (a) the Born-approximation cross sections [Formulas 3BN or 3BN(a)]; (b) the corrected Sauter-Fano cross sections at the high-frequency limit [Sec. IIE(2)]; (c) the Elwert-Born approximation cross sections [Sec. IIE(1)]; and (d) the experimental results. The solid lines show the cross sections computed from Formula 3BN(a) for 0.05 Mev, and Formula 3BN for

<sup>36</sup>N. Starfelt and H. W. Koch, Phys. Rev. **102**, 1598 (1956).

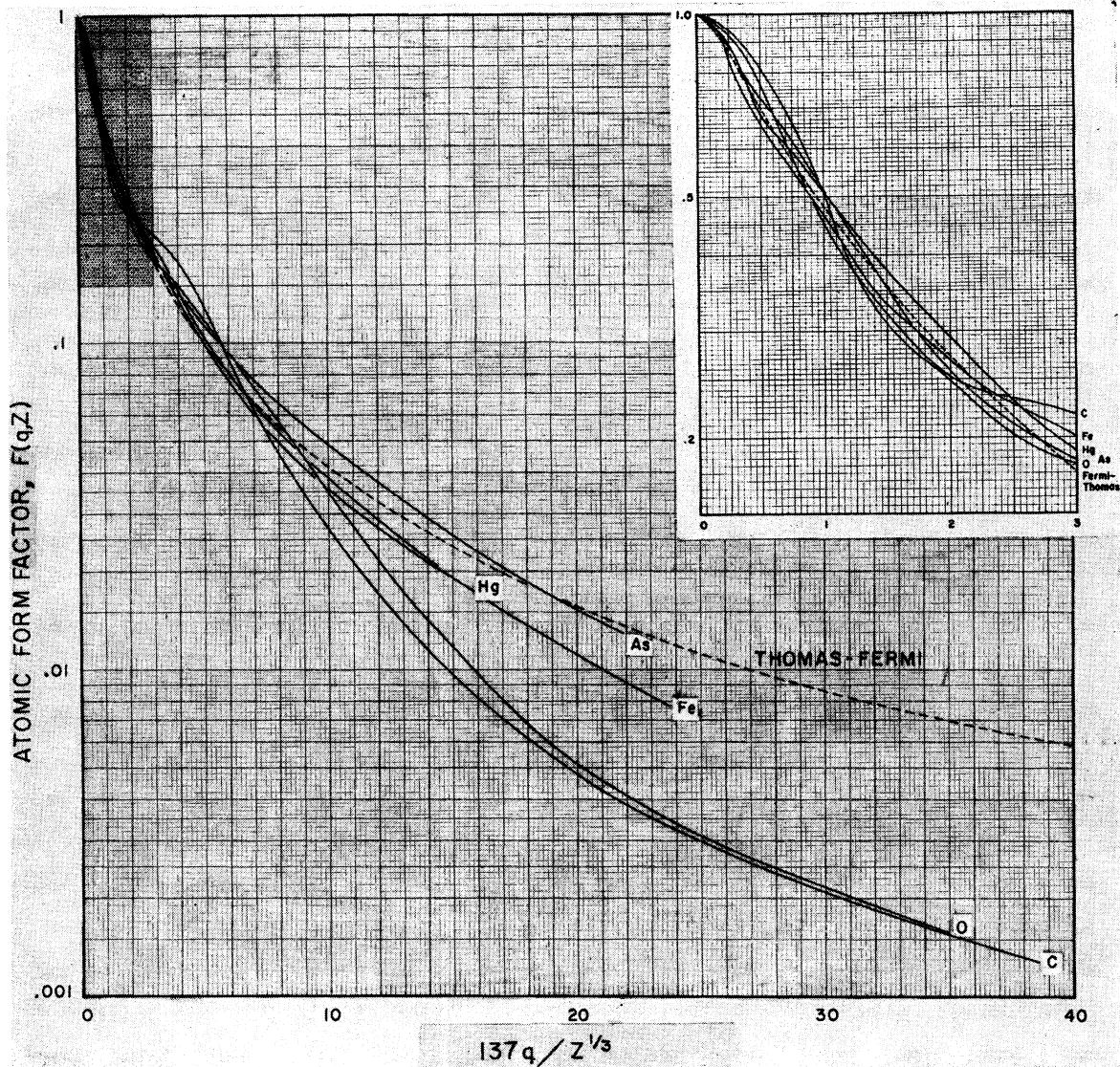


FIG. 14. Evaluation<sup>24</sup> of the atomic form factor,  $F(q,Z)$ , for the Hartree self-consistent field model (solid lines) and for the Thomas-Fermi model (dashed line), as a function of the nuclear momentum transfer,  $q$ .

0.5, 1, and 4.5 Mev. The dashed lines give the Born-approximation cross sections corrected by the Elwert factor defined in Formula (II-4). The comparison with the experimental results shows that the Elwert correction gives the most accurate results at very low energies (below 0.1 Mev). For electron kinetic energies of the order of the electron rest energy, the cross sections obtained with the Elwert correction factor are still less than the experimental values (by as much as a factor of two in the worst case). For very high energies, the Born-approximation theory overestimates the actual cross sections, and the Elwert factor is no longer valid, although it gives good agreement with experiment in the 5-Mev cross-over region [see Sec. IIF(3)]. The corrected Sauter-Fano cross sections at the high-frequency

limit show good agreement with the experimental results as noted previously in Fig. 12.

### (3) Total Cross Section

The experimental values for the total cross section,  $\phi_{rad}$  (defined in Sec. IIC), are shown in Fig. 22 by the closed and open circles for initial electron kinetic energies of 0.05 Mev,<sup>33</sup> 0.5 Mev,<sup>35</sup> and 1.0 Mev.<sup>35</sup> The theoretical values are shown by the solid lines, which are predicted by Formulas 4BN(a) in the region where  $T_0 \leq 0.5$  and by Formula 4BN for no screening. The curves that include screening corrections for  $Z=13$  and 79 are obtained by numerical integration of the intermediate screening Formulas 3BS(c) and 3BS(d). For

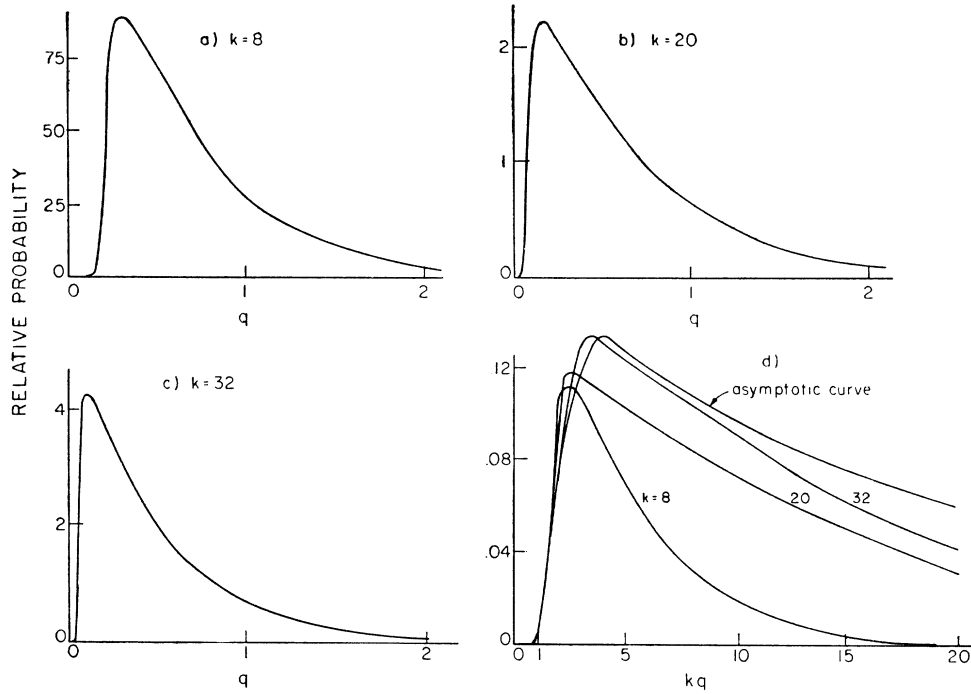


FIG. 15. Momentum distributions<sup>25</sup> for the recoil nucleus in nuclear pair production for several photon energies. The relative number of recoils are plotted in Figs. 15(a), (b), and (c) as a function of the momentum,  $q$ . These curves are summarized in (d) and are compared with the asymptotic curve.

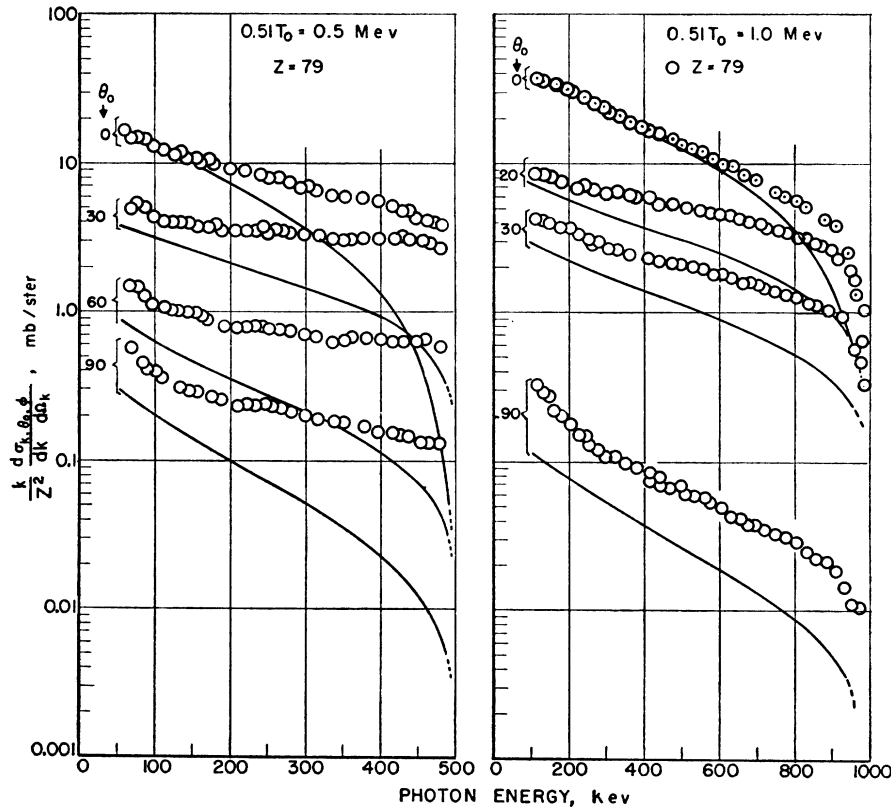


FIG. 16. Dependence of the bremsstrahlung cross section  $d\sigma_{k,\theta_0,\phi}$  on photon energy and angle,  $\theta_0$ , for 0.5- and 1.0-Mev electrons. The theoretical cross sections shown by the solid curves are calculated from Formula 2BN, and the experimental values<sup>26</sup> for gold are given by the open circles.

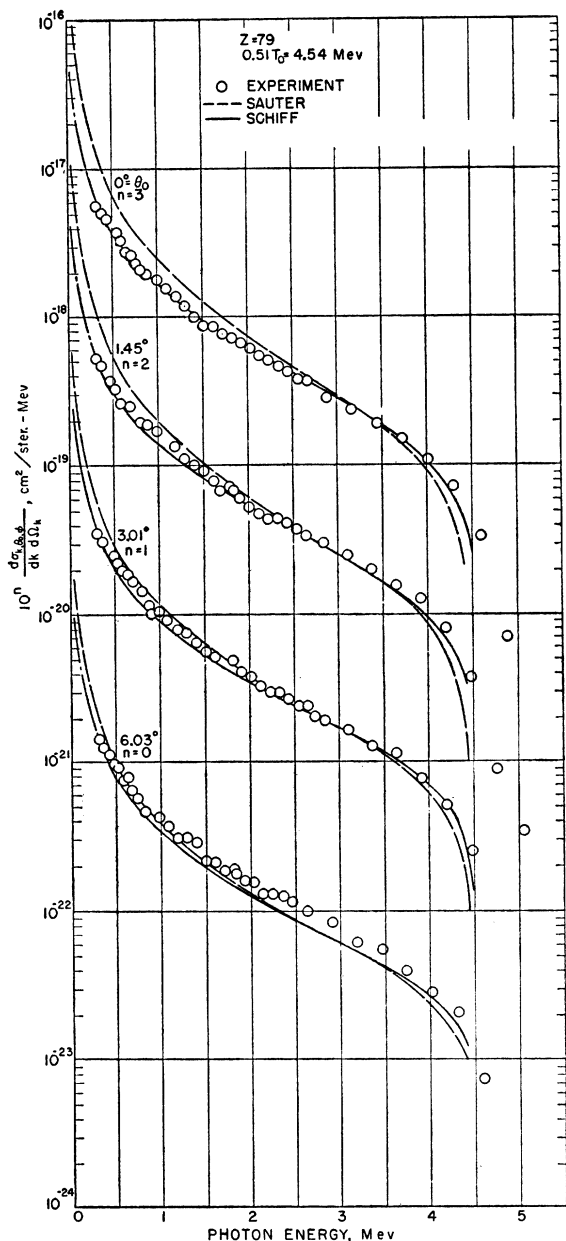


FIG. 17. Dependence of the bremsstrahlung cross section  $d\sigma_{k,\theta_0,\phi}$  for gold, on the photon energy and angle,  $\theta_0$ , for 4.54-Mev electrons. The theoretical cross sections are given by the solid curve (Schiff, Formula 2BS), and by the dashed curve (Sauter, Formula 2BN). The experimental values<sup>36</sup> for gold are given by the open circles.

extreme-relativistic energies, the triangles give the most accurate theoretical cross-section values<sup>37</sup> for  $Z=79$ , which are estimated by numerical integration of the Coulomb-corrected Formula 3CS. The most accurate values for  $\phi_{rad}$ , which are estimated from the

<sup>37</sup> For  $Z=13$ , the corrected values for energies above 50 Mev have only small differences (less than one percent) with the values shown by the solid line for  $Z=13$ .

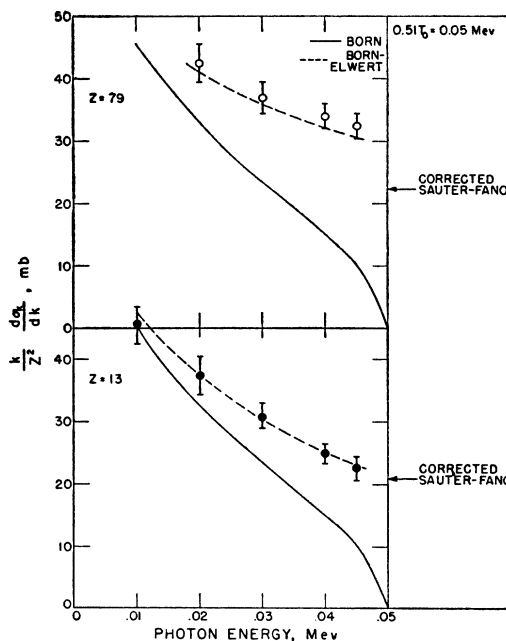


FIG. 18. Dependence of the bremsstrahlung cross section integrated over photon angle on the photon energy for 0.05-Mev electrons. The Born-approximation cross sections shown by the solid curves are calculated from Formula 3BN(a), and the Born-Elwert cross sections shown by the dashed curves are obtained from the product of Formula 3BN(a) and the Elwert factor, Formula (II-4). The experimental values<sup>38</sup> are shown by the open and closed circles for gold and aluminum, respectively. The corrected Sauter-Fano values at the high-frequency limit are estimated in reference 21.

above combined data, are shown by the dashed curve for  $Z=13$  and the dot-dashed curve for  $Z=79$ .

Approximate correction factors for the Born-approximation  $\phi_{rad}$  values with screening have been estimated as a function of the initial electron kinetic energy from the ratios of the cross-section values shown in Fig. 22 by the empirical (dashed and dot-dashed) curves and by the Born-approximation curves with screening. These estimated factors are given in Fig. 23, and show that the ratios are equal to unity at the energy of approximately 10 Mev for aluminum and 6 Mev for gold. For energies larger than these crossover energies, the Born-approximation formula overestimates the cross section; for smaller energies, the reverse is true. Even though the correction factor for  $\phi_{rad}$  may be close to unity for a given electron energy, much larger (or smaller) correction factors may be required for the differential cross section,  $d\sigma_k$ , in the high- or low-frequency region because of a crossover effect (see Fig. 39 in Bethe and Salpeter, reference 1), which is masked by the integration of  $d\sigma_k$ . It is interesting to observe in Fig. 23, that the maximum correction factor for the Born-approximation calculations occurs at electron kinetic energies approximately equal to the electron rest energy.

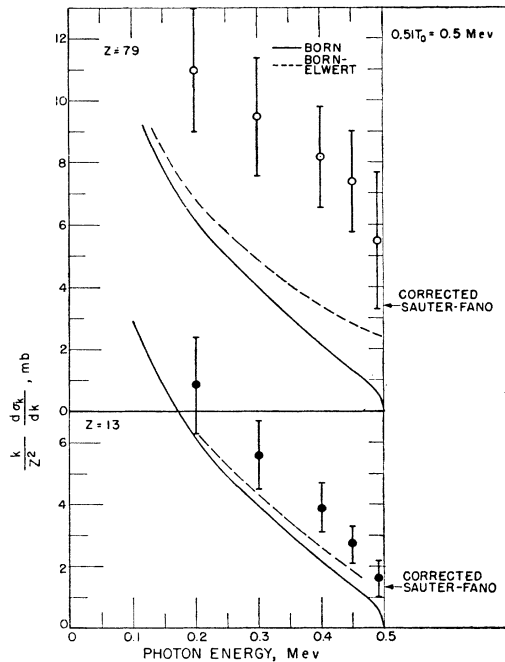


FIG. 19. Dependence of the bremsstrahlung cross section integrated over photon angle on the photon energy for 0.5-Mev electrons. The Born-approximation cross sections shown by the solid curves are calculated from Formula 3BN, and the Born-Elwert cross sections shown by the dashed curves are obtained from the product of Formula 3BN and the Elwert factor, Formula (II-4). The experimental values<sup>35</sup> are shown by the open and closed circles for gold and aluminum, respectively. The corrected Sauter-Fano values at the high-frequency limit are estimated in reference 21.

### G. Summary

A survey of the foregoing data leads to some general conclusions about the accuracy of the cross-section values predicted by the various formulas and correction factors. Also, suggestions can be made for selecting formulas that give the best estimates for the cross section or that can be easily evaluated to give reasonably accurate results. These judgments are summarized in the following.

In Table I, the screened formulas depend on the extreme-relativistic approximation and therefore are valid only in the energy region  $T_0 \gg 1$ . For  $T_0 \ll 1$ , only the nonscreened formulas are applicable.<sup>38</sup> The nonscreened formulas require relatively large correction factors except in the region near the crossover energy (see Fig. 22). At the extreme relativistic energies the nonscreened formulas are less accurate than the screened formulas.

In Table II, the extreme-relativistic cross section formulas for  $d\sigma_{k,\theta,\phi}$  and  $d\sigma_k$  are estimated to have an accuracy that is given approximately by the factor  $(Z/137)^2(\ln E/E)$ . For  $f(Z) = 0$ , the formulas in Table II

<sup>38</sup> A Born-approximation formula that includes screening effects without the extreme-relativistic approximation, has been given by Gluckstern and Hull, Phys. Rev. **90**, 1030 (1953). This formula applies mainly to the low-frequency region and has been found to be inadequate<sup>36</sup> in the high-frequency region.

are the same as the Born-approximation formulas in Table I except for differences in the screening corrections which are reviewed in Sec. III E(3).

An estimate of the general accuracy with which the formulas in Tables I and II predict the cross-section values over the whole range of electron energies can be obtained from a comparison of the theoretical and experimental predictions for  $\phi_{\text{rad}}$  in Figs. 22 and 23.

For the cross-section differential in photon energy,  $d\sigma_k$ , a summary of the corrected formulas for specified energy ranges of the incident electron is given in Table V. Conservative estimates of the accuracies of these

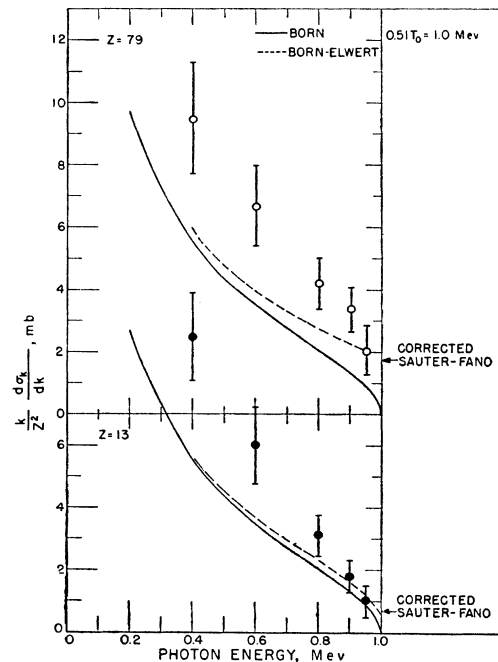


FIG. 20. Dependence of the bremsstrahlung cross section integrated over photon angle on the photon energy for 1.0-Mev electrons. The Born-approximation cross sections shown by the solid curves are calculated from Formula 3BN, and the Born-Elwert cross sections shown by the dashed curves are obtained from the product of Formula 3BN and the Elwert factor, Formula (II-4). The experimental values<sup>35</sup> are shown by the open and closed circles for gold and aluminum, respectively. The corrected Sauter-Fano values at the high-frequency limit are estimated in reference 21.

formulas have been made on the basis of the experimental data assembled in this report. The greatest uncertainties are in the energy range from 0.10 to 2.0 Mev. Because of the uncertainties of screening effects, no corrected formulas are given for the energy region below 0.1 Mev. These corrected formulas are tentative and it can be expected that some will be replaced by more accurate expressions as more data becomes available.

For the cross-section formulas differential in photon energy and angle,  $d\sigma_{k,\theta,\phi}$ , no quantitative corrections are available for low and intermediate energies because

of insufficient data. For extreme relativistic energies, the most accurate estimates (3%) for  $d\sigma_{k,\theta_0\phi}$  are given by Formula 2CS.

### III. ELECTRON-ELECTRON BREMSSTRAHLUNG

The bremsstrahlung cross-section formulas for electron-nuclear interactions in Sec. IIC vary as  $Z^2$ . For targets with high atomic numbers, the additional influence of electron-electron bremsstrahlung can be included approximately by replacing  $Z^2$  by  $Z(Z+1)$ . However for very low  $Z$  elements such as hydrogen or beryllium, the electron-electron bremsstrahlung contributions must be included more accurately. Cross-section calculations for this process are complicated because of the exchange character of the interaction in which there is a large energy and momentum transfer to the recoil electron, in contrast to the electron-nuclear bremsstrahlung proc-

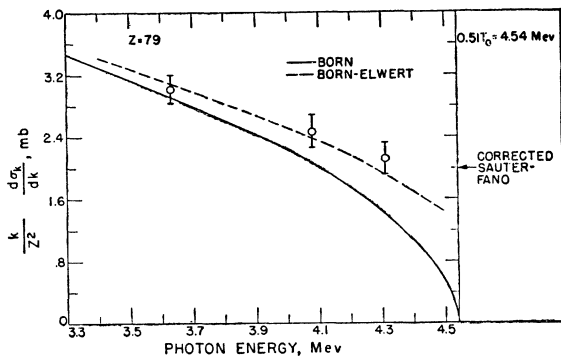


FIG. 21. Dependence of the bremsstrahlung cross section integrated over photon angle on the photon energy for 4.54-Mev electrons. The Born-approximation cross sections shown by the solid curve are calculated from Formula 3BN, and the Born-Elwert cross sections shown by the dashed curve are obtained from the product of Formula 3BN and the Elwert factor, Formula (II-4). The experimental values<sup>36</sup> are shown by the open circles for gold. The corrected Sauter-Fano values at the high-frequency limit are estimated in reference 21.

ess in which the nucleus is assumed to be infinitely heavy. No complete calculations are available for predicting the detailed features of electron-electron bremsstrahlung.<sup>39</sup> A summary of pertinent results that have been obtained is given in the following.

#### A. Maximum Photon Energy

In the electron-electron bremsstrahlung process, the maximum photon energy that is available in the laboratory system at the laboratory angle  $\theta_0$  is<sup>35</sup>

$$k_{\max} = F / (1 - \sqrt{F \cos \theta_0}), \quad (\text{III-1})$$

where  $F$  is equal to  $(E_0 - 1) / (E_0 + 1)$ . Table VI gives some values of  $k_{\max}$  at zero and 90 degrees obtained from Formula (III-1) for various incident electron kinetic

<sup>39</sup> For a general review of the available theories on electron-electron bremsstrahlung, see J. Joseph and F. Rohrlich, *Revs. Modern Phys.* **30**, 354 (1958).

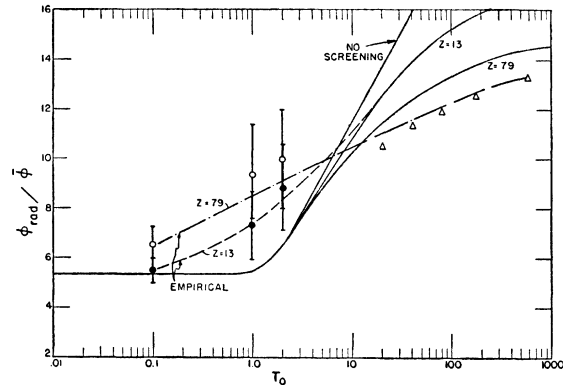


FIG. 22. Dependence of the total radiation cross section,  $\phi_{\text{rad}} [= (1/E_0) \int_0^{\theta_0} k d\sigma_k]$ , on the initial electron kinetic energy,  $T_0$ . The solid lines are obtained from Formula 4BN for no screening, and from the numerical integration of Formulas 3BS(c) and 3BS(d) with screening corrections for  $Z$  equal to 13 and 79. The experimental points<sup>35,36</sup> are shown by the open and closed circles for a gold and aluminum target, respectively. The values shown by the triangles are estimated by numerical integration of Formula 3CS for  $Z=79$ . On the basis of the experimental data at the low energies and the theoretical values (triangles) predicted by the exact theory at the extreme relativistic energies, the dashed curves have been drawn as an estimate of the most accurate  $\phi_{\text{rad}}$  values for  $Z$  equal to 13 and 79.

energies. From the very sparse experimental information<sup>35,36</sup> available on electron-electron bremsstrahlung, some results<sup>35</sup> have shown reasonably good agreement with the values of  $k_{\max}$  predicted by Formula (III-1).

### B. Cross-Section Formulas for Free Electrons

#### (1) Nonrelativistic Energies

In contrast to the electron-nucleus and electron-positron systems, the electron-electron system has no

TABLE V. Corrected cross-section formulas for  $d\sigma_k$ .

Kinetic energy range for incident electron, Mev	Corrected cross-section formula <sup>a</sup>	Restrictions	Estimated accuracy <sup>b</sup>
0.01-0.10	$d\sigma_k = f_B d\sigma_k^{3\text{BN}(a)}$	$k > 0.01T_0$	$\pm 5\%$
0.10-2.0	$d\sigma_k = A f_B d\sigma_k^{3\text{BN}}$	$k > 0.01T_0$	$\pm 20\%$
2.0-15	$d\sigma_k = A d\sigma_k^{3\text{BN}}$	$\gamma > 15$	b
	$= A d\sigma_k^{3\text{BS}(d)}$	$2 < \gamma < 15$	$\pm 5\%$
	$= A d\sigma_k^{3\text{BS}(e)}$	$\gamma < 2$	$\pm 5\%$
15-50	$d\sigma_k = d\sigma_k^{3\text{BN}}$	$\gamma > 15$	b
	$= A d\sigma_k^{3\text{BS}(d)}$	$2 < \gamma < 15$	$\pm 3\%$
	$= A d\sigma_k^{3\text{BS}(e)}$	$\gamma < 2$	$\pm 3\%$
50-500	$d\sigma_k = d\sigma_k^{3\text{BN}}$	$\gamma > 15$	b
	$= d\sigma_k^{3\text{CS}(a)}$	$2 < \gamma < 15$	$\pm 3\%$
	$= d\sigma_k^{3\text{CS}(b)}$	$\gamma < 2$	$\pm 3\%$

where  $f_B$  is defined in Formula (II-6),  $A$  is the correction factor given in Fig. 23,  $\gamma$  is equal to the quantity  $100k(E_0EZ)^{-1}$ .

<sup>a</sup> The superscripts for  $d\sigma_k$  give the formula numbers defined in Sec. IIC.  
<sup>b</sup> No estimated accuracy is given at photon energies near the high-frequency limit of the spectrum. If better accuracy is desired in this region, the cross section at the high-frequency limit can be obtained from the dashed curves in Fig. 12, and the spectrum shape may be adjusted by fitting this end to the curves given by the formulas in column 2 above.

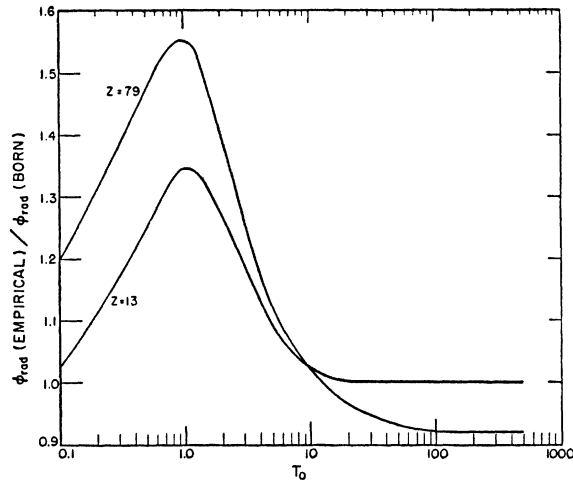


FIG. 23. Approximate correction factors for the Born-approximation  $\phi_{\text{rad}}$  values with screening shown in Fig. 22. These factors have been estimated from the ratios of the empirical (dashed and dot-dashed) curves to the Born-approximation curves with screening in Fig. 22.

dipole moment. Therefore the electron-electron bremsstrahlung cross section becomes zero for calculations based only on the nonrelativistic dipole approximation. Garibyan<sup>40</sup> has made calculations beyond the dipole approximation and has obtained the following non-vanishing result for the cross-section differential in photon energy:

$$d\sigma_k' = \frac{r_0^2 Z}{137} \left( \frac{8}{15} \frac{\beta}{\beta_0^3} \frac{dk}{k} \right) \left[ 17 - \frac{3(\beta_0^2 - \beta^2)^2}{(\beta_0^2 + \beta^2)^2} + \left( \frac{\beta_0^2 + \beta^2}{\beta_0 \beta} + 26 \frac{\beta_0 \beta}{\beta_0^2 + \beta^2} - \frac{24\beta_0^3 \beta^3}{(\beta_0^2 + \beta^2)^3} \right) \times \ln \left( \frac{\beta_0 + \beta}{\beta_0 - \beta} \right) \right], \quad (\text{III-2})$$

which for  $k \rightarrow 0$  becomes<sup>39</sup>

$$d\sigma_{k \rightarrow 0}' = \frac{r_0^2 Z}{137} \left[ \frac{32}{5} \frac{dk}{k} \frac{1}{\beta_0^2} \left( \ln \frac{4\beta_0^2}{k} + \frac{17}{12} \right) \right]. \quad (\text{III-3})$$

These results are only valid for  $T_0 \ll 1$ .

TABLE VI. Maximum photon energy for electron-electron bremsstrahlung.

$T_0$	$\theta_0 = 0^\circ$	$k_{\text{max}}$	$\theta_0 = 90^\circ$
100	99.		0.98
10	9.7		0.83
1.0	0.79		0.33
0.1	0.069		0.048
0.01	0.0054		0.0050

<sup>40</sup> G. M. Garibyan, Zhur. Eksptl. i Teoret. Fiz. 24, 617 (1953).

## (2) Extreme-Relativistic Energies

Several calculations<sup>39</sup> based on the extreme-relativistic approximations give the following approximate formula for the cross-section differential in photon energy:

$$d\sigma_k' = \frac{4r_0^2 Z}{137} \frac{dk}{k} \left[ \left( 1 + \left( \frac{E}{E_0} \right)^2 \right) \frac{2}{3} \frac{E}{E_0} \times \left( \ln \frac{2E_0 E}{k} - \frac{3}{2} \right) - \frac{E_0 E}{9} \right], \quad (\text{III-4})$$

which is similar in form to the electron-nuclear cross-section Formula 3BN(b).

The total radiation cross section obtained from For-

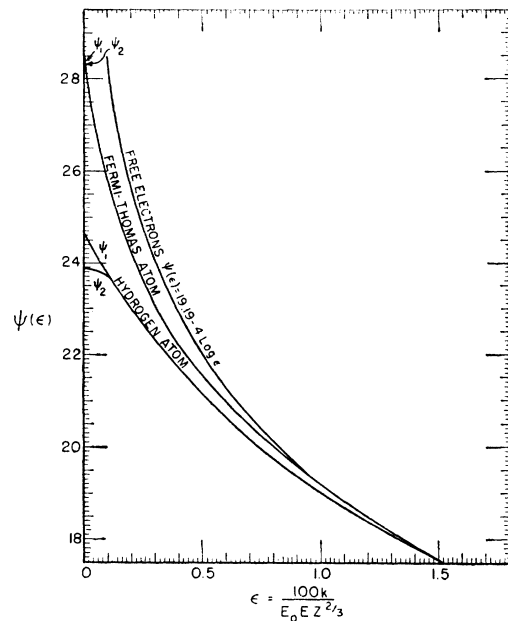


FIG. 24. Screening factors,<sup>41</sup>  $\psi_1$  and  $\psi_2$ , for electron-electron bremsstrahlung. The curve marked "Hydrogen atom" was calculated<sup>41</sup> with exact wave functions. For free electrons,  $\psi_1 = \psi_2 = \psi$ .

mula (III-4) is given as

$$\phi_{\text{rad}}' = \frac{4r_0^2 Z}{137} \left[ \ln(2E_0) - \frac{4}{3} \right]. \quad (\text{III-5})$$

## C. Cross-Section Formulas with Binding Corrections

The influence of atomic binding on the electron-electron bremsstrahlung cross section has been calculated only in the extreme-relativistic approximation. With the Thomas-Fermi model, the corrected formula for the cross-section differential in photon energy is<sup>39</sup>

$$d\sigma_k' = \frac{4r_0^2 Z}{137} \frac{dk}{k} \left[ \left( 1 + \left( \frac{E}{E_0} \right)^2 \right) \left( \frac{1}{4} \psi_1(\epsilon) - 1 - \ln Z^{\frac{1}{3}} \right) - \frac{2}{3} \frac{E}{E_0} \left( \frac{1}{4} \psi_2(\epsilon) - \frac{5}{6} - \ln Z^{\frac{1}{3}} \right) \right], \quad (\text{III-6})$$

where  $\epsilon$  is equal to  $100k(E_0EZ^{\frac{1}{2}})^{-1}$ , and  $\psi_1$  and  $\psi_2$  are given<sup>41</sup> by the data in Fig. 24. For complete screening where  $\epsilon \sim 0$ , the cross section becomes

$$d\sigma_{k'} = \frac{4r_0^2 Z}{137} \frac{dk}{k} \left( 1 + \left( \frac{E}{E_0} \right)^2 - \frac{2E}{3E_0} \right) \ln \frac{530}{Z^{\frac{1}{2}}}. \quad (\text{III-7})$$

The total radiation cross section which is obtained for the complete screening case from (III-7) is given by

$$\phi_{\text{rad}}' = (4r_0^2 Z / 137) \ln(530 / Z^{\frac{1}{2}}). \quad (\text{III-8})$$

A comparison of this Formula (III-8) with the electron-nuclear bremsstrahlung cross-section Formula 4BS shows that the  $Z$  electrons in an atom increase the electron-nuclear cross section by the factor  $\eta$  so that the total cross section becomes

$$\phi_{\text{rad}}^{\text{total}} = Z(Z + \eta) (\phi_{\text{rad}}^{\text{4BS}} / Z^2). \quad (\text{III-9})$$

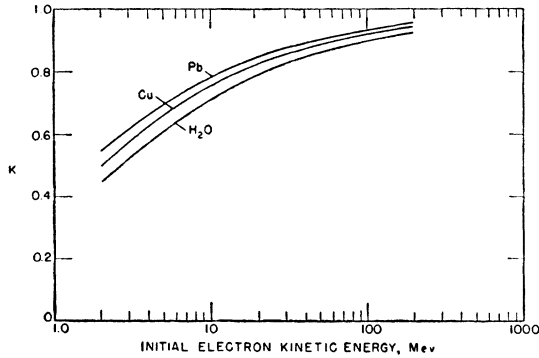


FIG. 25. Dependence of the radiation probability correction factor,  $K (= \phi_{\text{rad}} / \phi_{\text{rad}}^*)$ , on the initial electron kinetic energy and the target atomic number.

For complete screening,  $\eta$  is given by

$$\eta = \ln \frac{530}{Z^{\frac{1}{2}}} \left/ \left( \ln \frac{183}{Z^{\frac{1}{2}}} + \frac{1}{18} \right) \right., \quad (\text{III-10})$$

which varies from 1.04 for magnesium to 0.88 for lead. For most cases, a value of  $\eta$  equal to unity is sufficiently accurate.

#### IV. THICK-TARGET BREMSSTRAHLUNG PRODUCTION

Bremsstrahlung is produced in *thick* targets for most practical cases. In this discussion, a target is defined to be *thick* if the scattering and energy loss processes that occur as the electrons traverse the target have an appreciable influence on the bremsstrahlung production. In principle, a complete description of the bremsstrahlung emitted from a given target can be obtained from the cross sections for the pertinent elementary processes. For example, the angular distribution of the

total bremsstrahlung power, the shape of the bremsstrahlung spectrum from an x-ray tube, or the efficiency of bremsstrahlung production can be calculated if detailed data are available with regard to the bremsstrahlung and electron scattering (elastic and inelastic) processes. However, any such analysis is necessarily a complicated procedure, since the calculations for the energy loss and scattering of the primary electrons and the absorption of the x-rays in the target must be included with the cross-section information of Sec. II. Also, the analysis depends on the characteristics of a given experimental situation. For these reasons, this paper does not give a complete, systematic treatment of thick-target bremsstrahlung production; instead it is confined to the presentation of pertinent experimental data as well as useful analytical results and procedures. Also, emphasis is placed on thick-target results that give absolute data on photon intensities and bremsstrahlung production efficiencies.

Some of the analytical results for thick-target bremsstrahlung are most conveniently expressed in terms of certain quantities which are defined in the following discussion. When an electron traverses a target, the average energy lost in the path length element  $dx$  by radiation can be written as

$$-dE_0 = NE_0(K\phi_{\text{rad}}^*)dx = KE_0dt, \quad (\text{IV-1})$$

where  $N$  is the number of target atoms per  $\text{cm}^3$  and  $K\phi_{\text{rad}}^*$  is equal to the cross section  $\phi_{\text{rad}}$  defined in Sec. IIC.  $\phi_{\text{rad}}^*$  is equal to  $(4Z^2r_0^2/137) \ln(183Z^{-\frac{1}{2}}) \text{cm}^2$ , which is approximately the same as the expression for  $\phi_{\text{rad}}$  at extreme-relativistic energies (see Formula 4BS).  $K$  is defined as the radiation probability correction factor and is plotted in Fig. 25 for various values of the target atomic number and the electron kinetic energy. The length  $t$  is given in units of the radiation length,  $t_0$ , which is defined as

$$t_0 = 1 / N\phi_{\text{rad}}^* \text{cm}. \quad (\text{IV-2})$$

Values for  $t_0$  in units of  $\text{g}/\text{cm}^2$  as a function of the target atomic number are plotted in Fig. 26.

#### A. Thick-Target Bremsstrahlung Angular Distributions

##### (1) Nonrelativistic and Intermediate Energies<sup>42</sup>

For electron energies that are small or comparable to the electron rest energy, no analytical or empirical formulas have been derived for estimating the bremsstrahlung angular distribution from thick targets, and only a few experimental results are available.

In contrast to the extreme-relativistic region, the radiation intensity produced at these low energies is

<sup>42</sup> The results that are presented for the nonrelativistic and intermediate energy region where  $T_0 \leq 1$  apply only to targets that are thick enough to stop the electrons. For the relativistic region where  $T_0 \gg 1$ , there is no such restriction on the target thickness.

<sup>41</sup> J. A. Wheeler and W. E. Lamb, Phys. Rev. 55, 858 (1939), and 101, 1836 (1956).

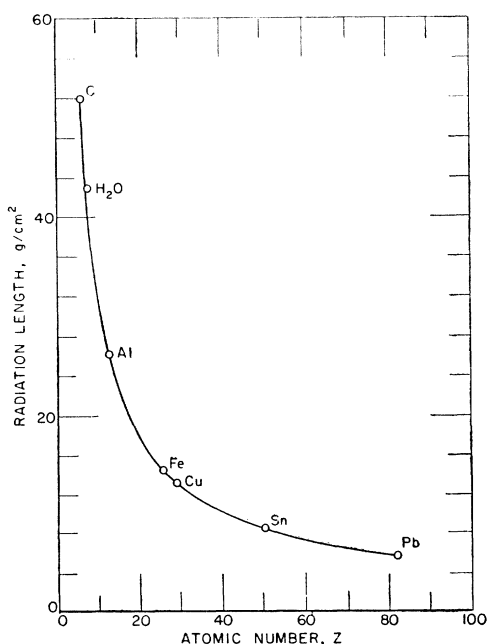


FIG. 26. Radiation lengths in grams per square centimeter for various materials.

important at large angles, and is about the same order of magnitude at both zero and ninety degrees. However, because the absorption of the bremsstrahlung photons in the target is large, the angular distribution of the bremsstrahlung is largely dependent on the target geometry in specific experimental situations. One of the few examples in which angular distribution data are presented in a more general way with corrections for the geometry and the target absorption is to be found in the measurements of Buechner, Van de Graaff, Burrill, and Sperduto<sup>43</sup> for initial electron kinetic energies in the region from 1.25 to 2.35 Mev. Their results for beryllium and gold targets are given in Fig. 27. The curves show the angular dependence of the radiation intensity integrated over photon energy for specified electron energies. These data indicate that the intensity ratio at zero and ninety degrees is approximately 10 for beryllium and 3 for gold at 1.5 Mev, and approximately 40 for beryllium and 4 for gold at 2.35 Mev. Also from these data, we can obtain the following empirical expressions for the power radiated at zero degrees:

$$I_{(\alpha=0)}(\text{Au}) = 9.4(\mathcal{T}_0)^{2.9} \text{ roentgens per minute per ma at 1 meter for gold,} \quad (\text{IV-3})$$

$$I_{(\alpha=0)}(\text{Be}) = 0.92(\mathcal{T}_0)^{3.4} \text{ roentgens per minute per ma at 1 meter for beryllium,}$$

where  $\mathcal{T}_0$  is the electron kinetic energy in  $m_0c^2$  units for the electrons incident on the target, and  $\alpha$  is the angle between the photon direction and the direction of the

<sup>43</sup> Buechner, Van de Graaff, Burrill, and Sperduto, Phys. Rev. 74, 1348 (1948).

incident electron beam. Then with the approximate conversion factor of one roentgen equal to  $3000 \pm 500$  ergs/cm<sup>2</sup> for photons with energies in the range from 0.1 to 2 Mev,<sup>44</sup> we have

$$I_{(\alpha=0)}(\text{Au}) = 0.5(\mathcal{T}_0)^{2.9} \text{ watts/ma-steradian,} \quad (\text{IV-4})$$

$$I_{(\alpha=0)}(\text{Be}) = 0.05(\mathcal{T}_0)^{3.4} \text{ watts/ma-steradian.}$$

From these equations, the fraction,  $R$ , of the total incident electron kinetic energy that is radiated per steradian at zero degrees is

$$R_{(\alpha=0)}(\text{Au}) = 10^{-3}(\mathcal{T}_0)^{1.9} \text{ for gold,} \quad (\text{IV-5})$$

and

$$R_{(\alpha=0)}(\text{Be}) = 10^{-4}(\mathcal{T}_0)^{2.4} \text{ for beryllium.}$$

## (2) Relativistic Energies

At high energies, estimates of the bremsstrahlung angular distribution from thick targets have been made on the basis of the following simplifying approximations. First, the thin-target spectrum integrated over photon angle (Formula 3BS) is assumed to represent the spectrum shape for any angle. Second, the intrinsic (thin target) angular spread of the bremsstrahlung (Formula 2BS) is neglected at large angles where  $\alpha \gg E_0^{-1}$  but not at small angles where  $\alpha \leq E_0^{-1}$ ; therefore, at large angles the photon is assumed to have the same direction as the electron that is multiply scattered before it radiates.

With these approximations, the following analytical results have been obtained. For large angles where  $\alpha \gg E_0^{-1}$ , the fraction,  $R$ , of the total incident electron

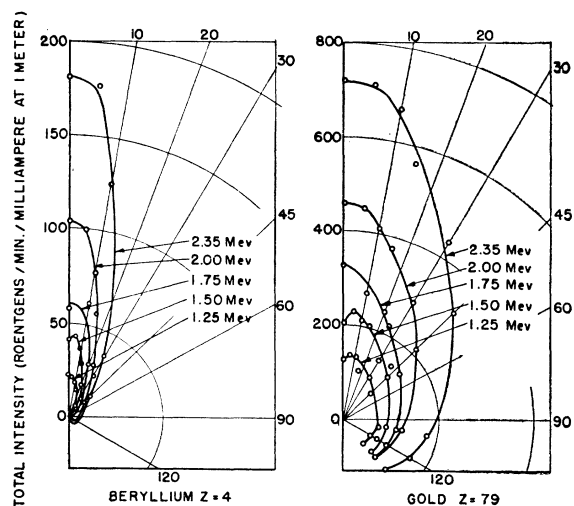


FIG. 27. Angular dependence of the thick-target bremsstrahlung intensity integrated over photon energy for 1.25- to 2.35-Mev electrons. These results were obtained by Buechner, Van de Graaff, Burrill, and Sperduto<sup>43</sup> and include corrections for the target.

<sup>44</sup> W. V. Mayneord, Brit. J. Radiol. Suppl. No. 2, 136 (1950). For photons outside this energy range, the conversion factor has a significant energy dependence and the factor must be weighted by the bremsstrahlung spectrum shape.

kinetic energy that is radiated per steradian at the angle,  $\alpha$ , is given<sup>45</sup> as

$$R(\alpha \gg E_0^{-1}) = \frac{K\mathcal{E}_0^2}{1760\pi} \text{Ei} \left[ \frac{-\mathcal{E}_0^2\alpha^2}{1760t} \right], \quad (\text{IV-6})$$

where  $\mathcal{E}_0$  is the total energy in  $m_0c^2$  units of the electron incident on the target, and Ei is the exponential integral<sup>46</sup>

$$-\text{Ei}(-y) = \int_y^\infty \frac{e^{-z}}{z} dz, \quad >0 \text{ for } y > 0. \quad (\text{IV-7})$$

For small angles where  $\alpha \lesssim E_0^{-1}$ , Muirhead, Spicer, and Lichtblau<sup>47</sup> have obtained the following expression for the bremsstrahlung angular distribution

$R(\alpha \lesssim E_0^{-1})$

$$= \frac{K\mathcal{E}_0^2}{1760\pi} \left\{ -\text{Ei} \left[ \frac{-\mathcal{E}_0^2\alpha^2}{1760t} \right] + \text{Ei} \left[ \frac{-\mathcal{E}_0^2\alpha^2}{7.15} \right] \right\}. \quad (\text{IV-8})$$

This formula gives good agreement with experimental data<sup>47</sup> and can readily be evaluated at small angles by keeping the first term in the expansion of the exponential integrals which is

$$\text{Ei}(-z_1) - \text{Ei}(-z_2) \rightarrow \ln(z_1/z_2) \text{ for } z_1, z_2 \rightarrow 0. \quad (\text{IV-9})$$

Thus

$$R_{(\alpha=0)} = \frac{K\mathcal{E}_0^2}{1760\pi} \ln 246t, \text{ for } t \gg 2 \times 10^{-3}. \quad (\text{IV-10})$$

For  $t=0.1$  and  $\mathcal{E}_0=3$ , this formula agrees reasonably well with the result predicted by the low-energy Formula (IV-5). For thin targets, this "on-axis" intensity becomes<sup>45</sup>

$$R_{(\alpha=0)} = Kt\mathcal{E}_0^2/4\pi, \text{ for } t \ll 2 \times 10^{-3}. \quad (\text{IV-11})$$

Estimates of the ratio  $R_\alpha/R_{(\alpha=0)}$  for tungsten ( $Z=74$ ) are given in Fig. 28 for three target thicknesses.

Several conclusions for high-energy angular distributions can be drawn from the form of the Formulas (IV-8), (IV-10), and (IV-11). The logarithmic form of Formula (IV-10) shows that most of the radiation comes from the front part of the target. Also, since the fractional energy radiated depends on  $\mathcal{E}_0^2$ , the total energy radiated at zero degrees will depend on  $\mathcal{E}_0^3$ . Two additional effects influence the dependence on  $\mathcal{E}_0$  of the total radiated energy. The factor  $K$ , according to Fig. 25, increases slightly with  $\mathcal{E}_0$ , and for very thick targets the effective  $t$  in Formula (IV-10) will increase loga-

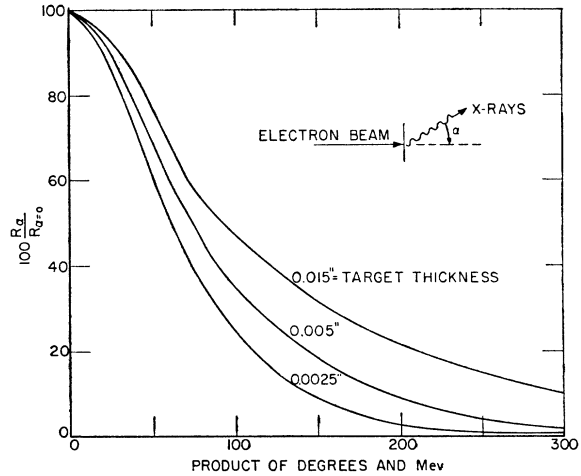


FIG. 28. Theoretical bremsstrahlung angular distributions from thick tungsten targets for relativistic energies. These data are obtained from the National Bureau of Standards Handbook 55.  $R_\alpha$  is defined as the fraction of the total incident electron kinetic energy that is radiated per steradian at the angle  $\alpha$ .

arithmically with  $\mathcal{E}_0$ . Therefore, the total energy radiated on the axis of the bremsstrahlung beam will depend on at least a 3.2 exponent for a thin target and on a slightly higher exponent for a thick target. The specific exponent to be used will depend on the energy range of interest, the effective target thickness, and the experimental geometry.

## B. Thick-Target Bremsstrahlung Spectra

### (1) Nonrelativistic and Intermediate Energies<sup>42</sup>

In this low-energy region the radiation has a broad angular distribution (see IVA), and the dependence of the spectrum shape on photon angle is important.<sup>48</sup> No general analytical expressions which accurately predict the spectrum as a function of angle for any experimental situation are available at these energies. Part of the difficulty has been the inadequacy of the Born-approximation cross-section differential in photon energy and angle (Formula 2BN). Nevertheless it has been possible to obtain reasonable agreement between theoretical and experimental thick-target spectrum shapes shown in Fig. 29 for a particular application<sup>49</sup> with an initial electron kinetic energy of 1.4 Mev, photon angles of zero and ninety degrees, and a tungsten target. In this example, the experimental results confirm the theoretical dependence of the spectrum shape on photon angle after distortions due to photon absorption in the target and surrounding materials are eliminated. The results also show that the relative number of photons in the high-frequency region increases as the emission angle becomes smaller. This trend is just opposite to the behavior observed for thin-target spectra.<sup>35</sup>

<sup>45</sup> J. D. Lawson, *Nucleonics* **10**, No. 11, 61 (1952).

<sup>46</sup> Exponential integral functions are tabulated in *National Bureau of Standards Tables of Sine, Cosine, and Exponential Integrals* (U. S. Government Printing Office, Washington, D. C.), Vols. 1 and 2 (MT5 and MT6).

<sup>47</sup> Muirhead, Spicer, and Lichtblau, *Proc. Phys. Soc. (London)* **A65**, 59 (1952).

<sup>48</sup> One of the earliest experimental indications of this dependence was found by C. E. Wagner, *Physik. Z.* **21**, 621 (1920).

<sup>49</sup> Miller, Motz, and Ciaella, *Phys. Rev.* **96**, 1344 (1954).

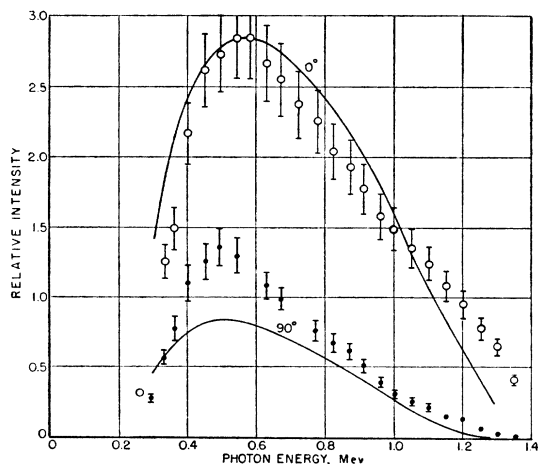


FIG. 29. Relative spectral intensities at  $0^\circ$  and  $90^\circ$  for 1.4-MeV electrons incident on a thick-tungsten target.<sup>49</sup> The solid curves are obtained from theoretical estimates that include electron scattering effects and photon absorption in the materials surrounding the target. The experimental values have been normalized and are shown by the open (zero degrees) and closed (90 degrees) circles. To obtain absolute spectral intensities in Mev per steradian per Mev per incident electron, the ordinate should be multiplied by  $10^{-3}$  for the theoretical curves and by  $2.1 \times 10^{-3}$  for the experimental points.

With regard to estimates of the shape of the spectrum integrated over the photon direction, Kramers<sup>50</sup> obtained the following simple, analytical expression:

$$I_k = AZ(k_0 - k), \quad (\text{IV-12})$$

where  $I_k$  is the energy radiated in all directions in the energy interval,  $(k, k+dk)$ ,  $A$  is a proportionality constant, and  $k_0$  is the photon energy at the high-frequency limit. This result was derived on the basis of a nonrelativistic, semiclassical calculation, in which electron scattering effects (including backscattering) were neglected and only the electron energy loss was considered. In spite of these limitations and because of its simplicity, the Kramers Formula (IV-12) has been used extensively to estimate the thick-target spectrum (not including the characteristic radiation<sup>51</sup>) at a given angle for various experimental cases, with corrections included for the photon absorption in the target and surrounding materials. Results obtained for various electron energies in this low-energy region have shown general qualitative agreement between the theoretical (Kramers) and experimental spectrum shapes,<sup>52</sup> and indicate that Formula (IV-12) is satisfactory, at least for order of magnitude estimates.

<sup>50</sup> H. A. Kramers, *Phil. Mag.* **46**, 836 (1923).

<sup>51</sup> For estimates of the thick-target characteristic radiation intensities that are superimposed on the continuous spectrum, see A. H. Compton and S. K. Allison, *X-Rays in Theory and Practice* (D. Van Nostrand Company, Inc., Princeton, New Jersey, 1949), pp. 69-89.

<sup>52</sup> A detailed summary of such comparisons is given in *Natl. Bur. Standards (U.S.) Handbook 62*, 20-24 (1957).

## (2) Relativistic Energies<sup>42</sup>

Two complementary procedures for calculating thick-target spectra at high energies which include effects of electron scattering in the target are given by Penfold<sup>53</sup> and Hisdal.<sup>54</sup> The Penfold calculations estimate the thick-target effects primarily in the high-frequency region and give the spectrum integrated over photon directions up to a maximum angle,  $\Gamma$ , with respect to the direction of the incident electron beam. The Hisdal calculations estimate the thick-target effects on the over-all spectrum shape in the forward direction and should not be applied to the high-frequency region.

The Penfold method<sup>53,55</sup> assumes that (a) the Schiff Formula 3BS(e) describes the intrinsic spectrum at all angles; (b) the electron energy loss rather than electron scattering in the target produces the predominant effect on the shape of the spectrum for large values of  $\Gamma$ ; (c) no electron radiates more than one photon; and (d) the photon absorption in the target is negligible. With these approximations, Penfold obtained the following formula for the thick-target spectrum integrated over photon direction to a maximum angle  $\Gamma$  determined by the detector:

$$P_k = nN_0 \int_{k+1}^{\epsilon_0} S(\mathcal{E}_0, E_0, \Gamma, x_0) d\sigma_k dE_0, \quad (\text{IV-13})$$

where  $P_k$  is the number of photons in the energy interval  $k$  to  $k+dk$ ,  $N_0$  is the number of target atoms per  $\text{cm}^3$ ,  $n$  is the number of electrons incident on the target,  $\mathcal{E}_0$  is the total energy of the incident electron in  $m_0c^2$  units,  $x_0$  is the target thickness in  $\text{g}/\text{cm}^2$ , and  $d\sigma_k$  is given by Formula 3BS(e) for electrons with energy  $E_0$ . The function  $S$  represents the probability that radiation produced by the electrons reaches the detector, and can be written as

$$S(\mathcal{E}_0, E_0, \Gamma, x_0) = \int_0^{x_0} B_3(\mathcal{E}_0, E_0, \Gamma, x) B_4(\Gamma, E_0, x) B_5(x_0, x) dx, \quad (\text{IV-14})$$

where the function  $B_3$  gives the fraction of the radiation emitted by electrons with energy  $E_0$  at the target depth  $x$ ,  $B_4$  is the fraction of electrons that penetrate beyond the thickness  $x$ , and  $B_5$  accounts for path length straggling. These  $B$  functions require involved numerical evaluations, and the results are described in detail in the Penfold report.<sup>53</sup> Motz, Miller, and Wyckoff<sup>56</sup> have estimated the thick-target spectrum for a particular experimental situation in which the brems-

<sup>53</sup> A. Penfold, University of Illinois Report (unpublished).

<sup>54</sup> E. Hisdal, *Phys. Rev.* **105**, 1821 (1957); E. Hisdal, *Arch. for Math. Naturvidenskab* **54**, No. 3, 1 (1957).

<sup>55</sup> A similar but less general method has been used by R. Wilson, *Proc. Phys. Soc. (London)* **A66**, 638 (1953). Wilson's calculations did not include electron scattering effects in the target and his results give a spectrum shape averaged over the photon directions.

<sup>56</sup> Motz, Miller, and Wyckoff, *Phys. Rev.* **89**, 968 (1953).

strahlung is produced with an 11.3 Mev (kinetic energy) electron beam incident on a tungsten target (approximately 0.010-inch thick), and is measured on the beam axis with a small detector ( $\Gamma \sim 0$ ). They used the following simplified, analytical form for the thick-target generating function:

$$S = 1 - \exp \left\{ -\frac{1}{51(\mathcal{E}_0 - E_0)} \left( \frac{\mathcal{E}_0}{E_0} \right)^2 \right\} \quad (\text{IV-15})$$

and, as shown in Fig. 30, have obtained good agreement with experimental results. For the more general calculations, Penfold used Formulas (IV-13) and (IV-14) to estimate the thick-target spectrum shapes for an incident electron kinetic energy of 15 Mev, a 0.020-inch platinum target, and for two detectors which subtend different angles on the electron beam axis, ( $\Gamma = 10$  degrees,  $\Gamma \gg 10$  degrees). A comparison is made in Fig. 31 of these two Penfold results (curves C and D) with the spectrum shape predicted by Formula 3BS(e) (curve A) and with the shape resulting from the application of the  $S$  function in Formula (IV-15) (curve B). The curves show that Formulas 3BS(e) and (IV-15) give a greater number of photons in the high-frequency region relative to the total number in the spectrum compared with the more accurate spectral shape predicted by the Penfold procedure. For certain cases, the spectrum shape predicted by the simplified Formula (IV-15) may be sufficiently accurate.

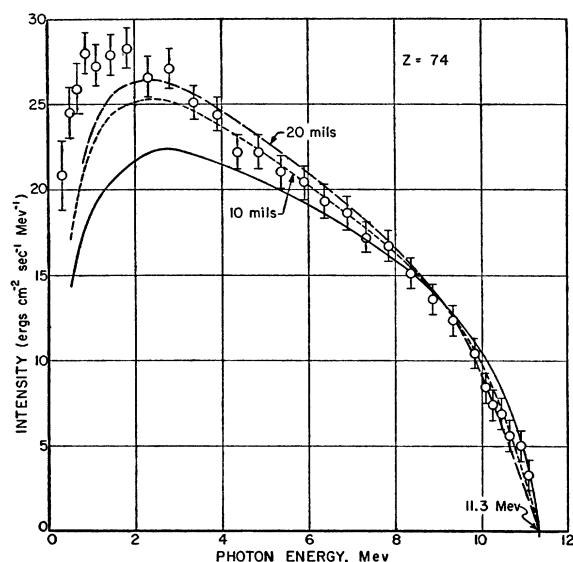


FIG. 30. Bremsstrahlung intensity spectrum in the forward direction for 11-Mev electrons incident on a thick-tungsten target.<sup>56</sup> The thin-target Born spectrum, modified by the photon absorption in the materials surrounding the target, is shown by the solid curve. The dashed curves show the spectra expected for a 10-mil and a 20-mil target, and the experimental values are given by the open circles.

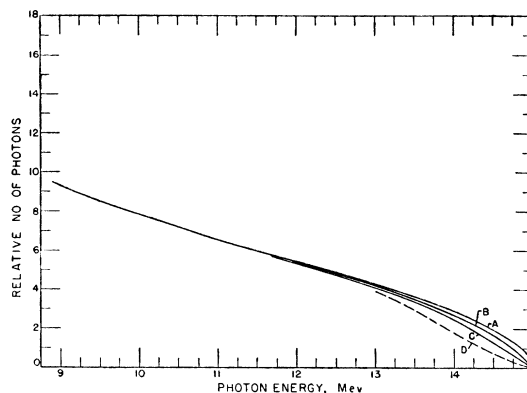


FIG. 31. Comparison of the spectrum shapes predicted by the thick target Penfold calculations<sup>58</sup> and by Schiff's thin target Formula 3BS(e) for 15-Mev electrons. The Schiff curve *A* shows the spectrum integrated over photon angle. Curve *B* is the spectrum shape predicted by Formula (IV-13) with the simplified  $S$  function given by Formula (IV-15). Curve *C* is the spectrum shape predicted by the Penfold calculations [Formulas (IV-13) and (IV-14)] for a 0.020-in. platinum target and a detector which subtends an angle,  $\Gamma$ , of 10 degrees. Curve *D* gives the Penfold spectrum for  $\Gamma \gg 10$  degrees.

The Hisdal method<sup>57</sup> assumes that (a) the spectrum variation with angle as given by the Schiff Formula 2BS has the dominant effect on the thick-target spectrum shape; (b) the energy loss of electrons in the target is negligible; (c) no electron radiates more than one photon; and (d) the photon absorption in the target is negligible. With these approximations, Hisdal has calculated tables for estimating the spectrum shape to be expected in a small detector placed on the electron beam-target axis. Hisdal's results are given in terms of a correction factor which multiplies Formula 3BS(e) for a given value of  $k$  to obtain the corrected spectrum for a particular target thickness. Examples of spectra calculated by Hisdal's method are given in Figs. 32(a)-(e) for 10-, 20-, 40-, 90-, and 300-Mev electrons, and are compared with the Schiff spectra integrated over photon direction [Formula 3BS(e)]. When the detector subtends a large solid angle at the target, the measured spectrum shape is given by the cross section integrated over the photon direction. Figures 7 and 8 give data for the spectrum shape included within a given detector angle. If this shape for a given experimental arrangement is estimated to be similar to the zero degree spectrum, then the Hisdal correction will be important; if this shape is estimated to be more similar to the spectrum integrated over all angles, then Hisdal's correction will be unimportant.

### C. Efficiency for Bremsstrahlung Production

The bremsstrahlung production efficiency for a given electron kinetic energy and target material is defined

<sup>57</sup> Similar calculations that apply only to a specific target material and electron energy have been made by A. Sirlin, *Phys. Rev.* **106**, 637 (1957). While the Hisdal calculations include only the Schiff complete screening approximations, Sirlin examined the effects of both the intermediate and complete screening approximations on the spectrum shape.

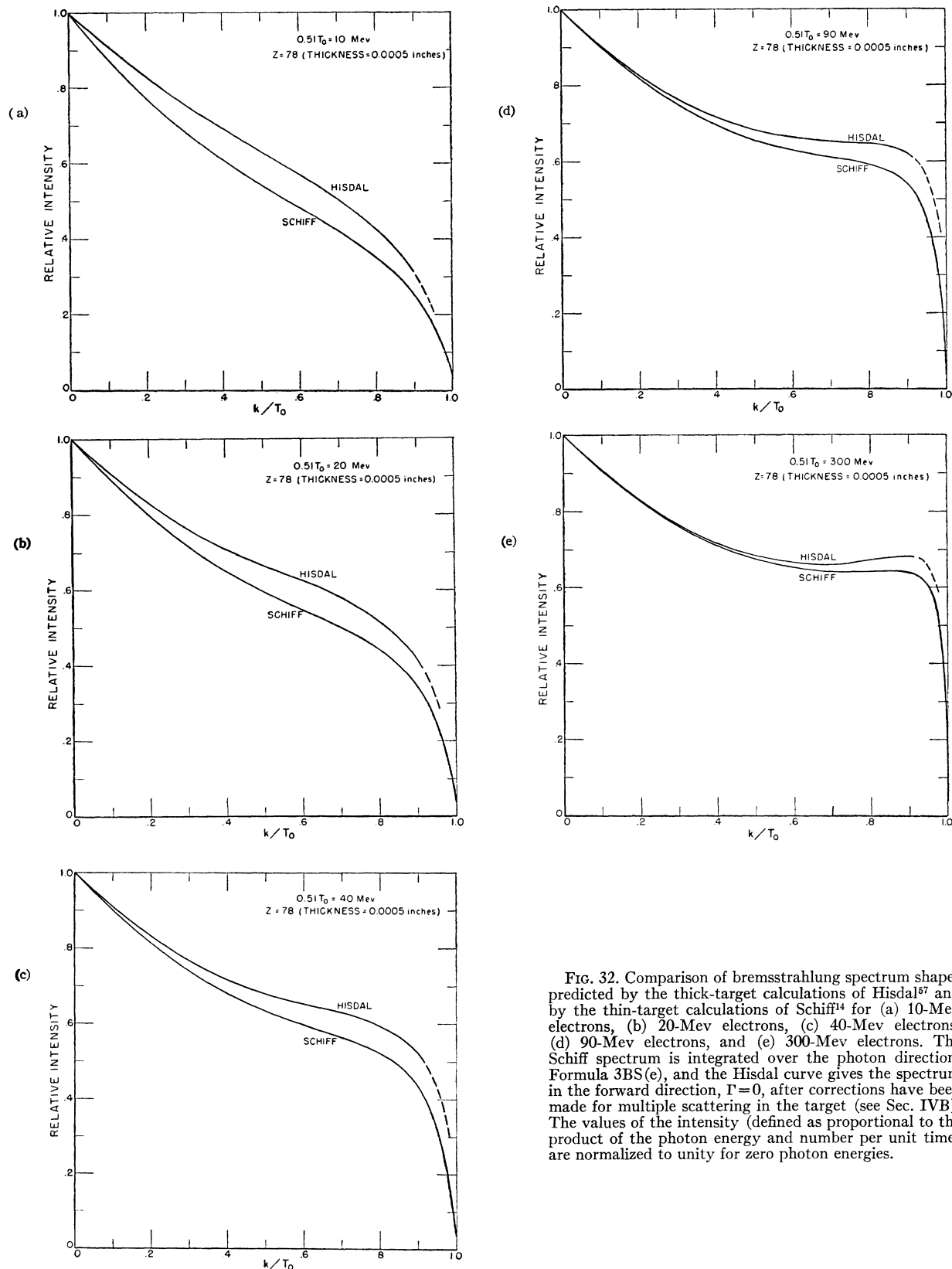


FIG. 32. Comparison of bremsstrahlung spectrum shapes predicted by the thick-target calculations of Hisdal<sup>57</sup> and by the thin-target calculations of Schiff<sup>14</sup> for (a) 10-Mev electrons, (b) 20-Mev electrons, (c) 40-Mev electrons, (d) 90-Mev electrons, and (e) 300-Mev electrons. The Schiff spectrum is integrated over the photon direction, Formula 3BS(e), and the Hisdal curve gives the spectrum in the forward direction,  $\Gamma=0$ , after corrections have been made for multiple scattering in the target (see Sec. IVB). The values of the intensity (defined as proportional to the product of the photon energy and number per unit time) are normalized to unity for zero photon energies.

as the ratio of the total bremsstrahlung power radiated when an electron current is incident on a target to the total power in the incident electron beam. The results of various theoretical and experimental determinations of the efficiency are given in the following.

(1) *Nonrelativistic and Intermediate Energies*

The efficiency results for this energy region apply only to the cases in which the electrons expend all of their kinetic energy in the target. Experimental determinations are complicated by (a) the large photon absorption in the target and (b) the large electron back-scattering from the target.<sup>49</sup> In the available measurements of the efficiency, corrections have been made for effect (a) but not for effect (b). Therefore, these experimental efficiencies are less than the values that would be obtained if all of the electrons were completely stopped in the target.

In this low-energy region, most experimental and theoretical results<sup>58</sup> are in agreement within a factor of two with an efficiency,  $\epsilon$ , given by the following formula:

$$\epsilon = 5 \times 10^{-4} Z T_0. \quad (\text{IV-16})$$

(2) *Relativistic Energies*

(a) *Intermediate thickness targets.*—A target is defined to have an intermediate thickness if the incident electrons do not expend all of their energy as they traverse the target. This condition usually exists in high-energy electron accelerators.

The efficiency of bremsstrahlung production for targets having an intermediate or small ( $\ll t_0$ ) thickness can be estimated from the expression

$$\epsilon = [(d\mathcal{E}_0)_R / T_0] \sim Kt, \quad (\text{IV-17})$$

where  $(d\mathcal{E}_0)_R$  is the energy loss by radiation,  $t$  is the target thickness in units of the radiation length  $t_0$  [Formula (IV-2)] and  $K$  is the radiation probability correction factor given in Fig. 25.

(b) *Thick targets.*—For thick targets, the incident electrons lose all of their energy in the target. Formula (IV-16) obviously does not apply at high energies for which the efficiency must remain less than one. An approximate relation for the efficiency in this high energy region has been derived<sup>59</sup> by assuming that the total electron energy loss per unit path length can be

<sup>58</sup> These results are summarized by H. Kulenkampff, "Physics of the Electron Shells," *Fiat Rev. Ger. Sci.* **1939-1946**, 95; R. D. Evans, *The Atomic Nucleus* (McGraw-Hill Book Company, Inc., New York, 1955), p. 616; and by S. T. Stephenson (reference 1).

<sup>59</sup> H. W. Koch and J. W. Wyckoff, *IRE Trans. on Nuclear Sci. NS-5*, No. 3 (1958).

TABLE VII. Approximate percentage efficiencies for x-ray production.

$T_0$ :	2	4	10	20	50	600
Carbon	0.36	0.72	1.77	3.47	8.3	52
Aluminum	0.77	1.54	3.75	7.2	16.3	70
Iron	1.54	3.0	7.2	13.5	28.1	82
Lead	4.7	9.0	19.7	33	55	94

written as

$$-\frac{d\mathcal{E}_0}{dx} = -\left(\frac{\rho Z}{A}\right)\{6 + 3.5 \times 10^{-3} \mathcal{E}_0 Z\}, \quad (\text{IV-18})$$

where  $\rho$  is the density and  $A$  the atomic weight of the target material, and where the first term is the collision loss and the second term is the radiation loss. Integration from the initial energy  $\mathcal{E}_0$  to 1 gives the following distance,  $x_0$ , traveled by an electron in losing all of its energy:

$$x_0 = \frac{A}{3.6 \times 10^{-3} \rho Z^2} \ln(1 + 6 \times 10^{-4} Z \mathcal{E}_0). \quad (\text{IV-19})$$

Then the efficiency becomes

$$\begin{aligned} \epsilon &= 1 - \frac{\text{collision loss}}{\mathcal{E}_0} = 1 - \frac{6\rho Z x_0}{A \mathcal{E}_0} \\ &= \frac{3 \times 10^{-4} Z T_0}{1 + 3 \times 10^{-4} Z T_0}. \end{aligned} \quad (\text{IV-20})$$

This procedure does not account for the large fluctuations in the radiation loss process and, therefore, provides only a rough estimate of the efficiency. At low energies, Formula (IV-20) reduces to  $3 \times 10^{-4} Z T_0$ , which agrees roughly with Formula (IV-16). Some representative values of the efficiency obtained from Formula (IV-20) are given in Table VII. These values do not include corrections for the x-ray absorption in the target, which cannot be neglected for most situations.

## V. ACKNOWLEDGMENTS

This report has benefitted considerably from discussions with Dr. U. Fano, Dr. M. Danos, Dr. J. Leiss, and Dr. H. O. Wyckoff. We are grateful to them for their helpful comments and criticisms. We express our special thanks to Dr. L. Maximon who critically reviewed the manuscript and made available a paper by Olsen and Maximon prior to publication. We are also indebted to Mr. John Hubbell for the comparison of the Hisdal and Sirlin results and for most of the computations and detailed plotting in the figures.

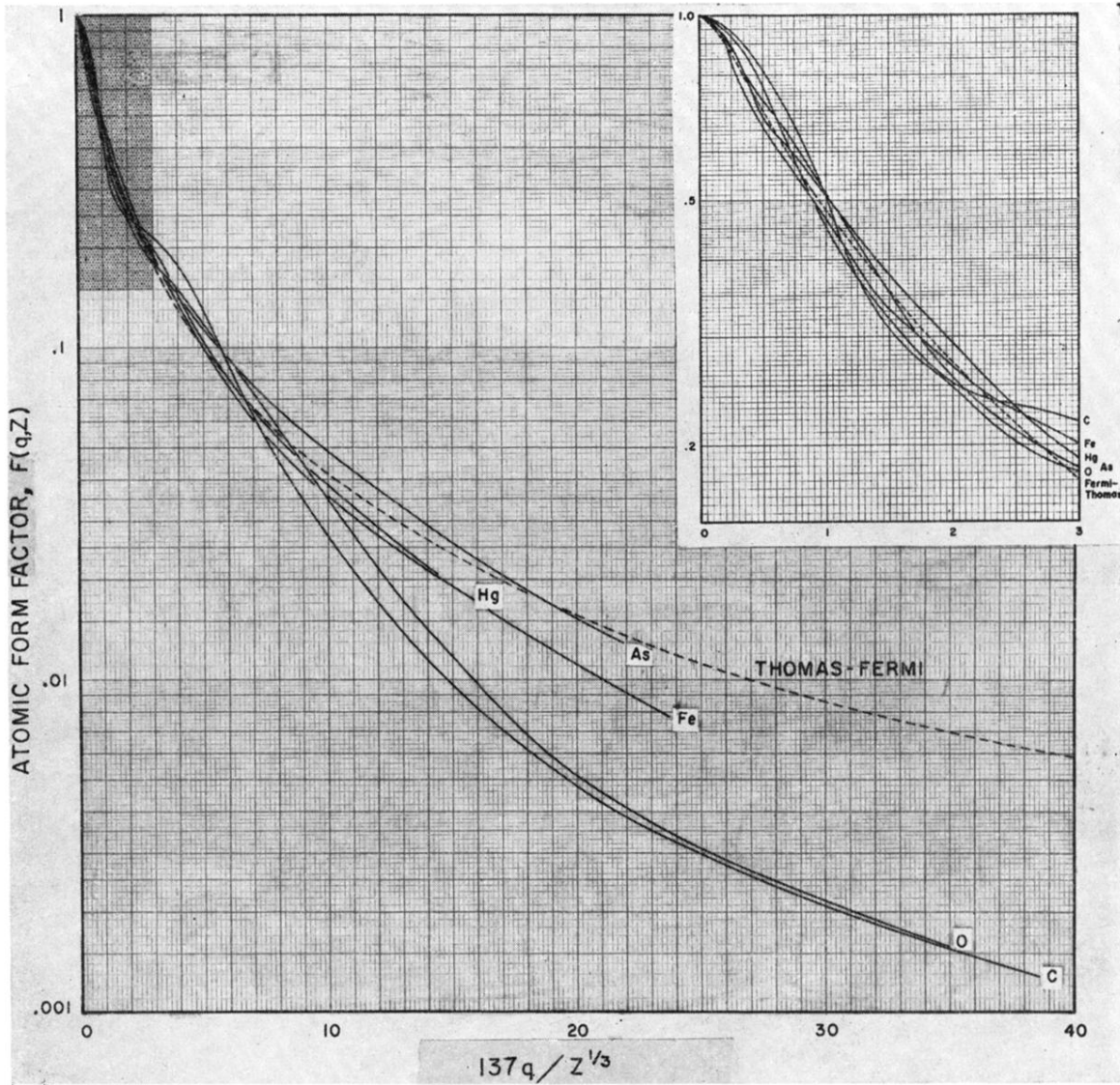


FIG. 14. Evaluation<sup>24</sup> of the atomic form factor,  $F(q,Z)$ , for the Hartree self-consistent field model (solid lines) and for the Thomas-Fermi model (dashed line), as a function of the nuclear momentum transfer,  $q$ .